A stable microtubule array drives fission yeast polarity reestablishment upon quiescence exit

Damien Laporte, Fabien Courtout, Benoit Pinson, Jim Dompierre, Bénédicte Salin, Lysiane Brocard, Isabelle Sagot

Published June 29, 2015

A stable microtubule array drives fission yeast polarity reestablishment upon quiescence exit

Damien Laporte,[1,2] Fabien Courtout,[1,2] Benoît Pinson,[1,2] Jim Dompierre,[1,2] Bénédicte Salin,[1,2] Lysiane Brocard,[3] and Isabelle Sagot[1,2]

[1]Université de Bordeaux, Institut de Biochimie et Génétique Cellulaires, 33000 Bordeaux, France
[2]Centre National de la Recherche Scientifique, UMR5095 Bordeaux, 33077 Bordeaux, France
[3]Bordeaux Imaging Center, Pôle d'imagerie du végétal, Institut National de la Recherche Agronomique, 33140 Villenave d'Ornon, France

Cells perpetually face the decision to proliferate or to stay quiescent. Here we show that upon quiescence establishment, *Schizosaccharomyces pombe* cells drastically rearrange both their actin and microtubule (MT) cytoskeletons and lose their polarity. Indeed, while polarity markers are lost from cell extremities, actin patches and cables are reorganized into actin bodies, which are stable actin filament–containing structures. Astonishingly, MTs are also stabilized and rearranged into a novel antiparallel bundle associated with the spindle pole body, named Q-MT bundle. We have identified proteins involved in this process and propose a molecular model for Q-MT bundle formation. Finally and importantly, we reveal that Q-MT bundle elongation is involved in polarity reestablishment upon quiescence exit and thereby the efficient return to the proliferative state. Our work demonstrates that quiescent *S. pombe* cells assemble specific cytoskeleton structures that improve the swiftness of the transition back to proliferation.

Introduction

Microtubules (MT) are hollow cylindrical polymers that are essential in all eukaryotic cells. They are formed by the non-covalent interaction of α- and β-tubulin heterodimers. MTs are nucleated at MT organizing centers (MTOCs) by a γ-tubulin–containing complex that acts as a MT template. As a MTOC stays attached to MT, it stabilizes the so-called MT minus end (Kollman et al., 2011). At the opposite end, the plus end, MTs elongate by the addition of GTP tubulin. During assembly, the β-tubulin–bound GTP is hydrolyzed and a stable GDP+Pi tubulin intermediate is generated. The eventual Pi release causes a change in tubulin–tubulin interaction that favors MT depolymerization (catastrophe) that can be rescued by de novo GTP tubulin addition (Carlier and Pantaloni, 1981; Nogales and Wang, 2006; Alushin et al., 2014; Mitchison, 2014). In fact, MT plus ends are thought to be protected from catastrophe by a stabilizing GTP tubulin "cap" (Mitchison and Kirschner, 1984; Horio and Murata, 2014). Thus, MTs alternate periods of growth and shrinkage, a behavior called dynamic instability (Mitchison and Kirschner, 1984). In vivo, this dynamic is regulated by plethora of MT-associated proteins (MAPs) that modulate MT length by influencing the polymerization or depolymerization rates and/or the catastrophe or rescue frequencies (Wade, 2009; van der Vaart et al., 2009; Horio and Murata, 2014). Finally, other MAPs are involved in MT organization into diverse structures such as asters, spindles, or bundles, each of which is required for a particular cellular process. One of the key questions is therefore how cells can spatially and temporally control the assembly of distinct MT-containing structures to elicit specific cellular functions.

Fission yeast has proven to be a powerful model to study how different MT structures are constructed all along the cell cycle (Hagan, 1998). Depending on the cell cycle stage, *Schizosaccharomyces pombe* displays three different classes of MTOCs. In mitosis, the spindle pole body (SPB), a yeast MTOC equivalent to the centrosome, nucleates MTs that form the mitotic spindle required for chromosome segregation. After mitosis completion, an equatorial MTOC appears as a ring in the cell center and nucleates a post-anaphase array of MTs involved in cell septation during cytokinesis. After cell division, the equatorial MTOC breaks down to form multiple interphase MTOCs that localize all around the nuclear membrane. The SPB stays linked to the cytoplasmic face of the nuclear envelope and can possibly nucleate interphase MT. Thus, in interphase, fission yeast cells display three to five long MT bundles that extend along the long axis of the cell (Hagan and Petersen, 2000; Sawin and Tran, 2006).

Interphase MT bundles are composed of about four dynamic antiparallel MTs (Drummond and Cross, 2000). The formation of these structures relies on the Mto1/2 complex that recruits and activates the γ-tubulin–containing complex on the

Correspondence to Isabelle Sagot: isabelle.sagot@ibgc.cnrs.fr

Abbreviations used in this paper: CHX, cycloheximide; MAP, MT-associated protein; MBC, benzimidazol-2-yl-carbamate; MPA, mycophenolic acid; MT, microtubule; MTOC, MT organizing center; SPB, spindle pole body; TBZ, thiabendazole; WT, wild type.

Supplemental Material can be found at:
http://jcb.rupress.org/content/suppl/2015/06/26/jcb.201502025.DC1.html

The Rockefeller University Press $30.00
J. Cell Biol. Vol. 210 No. 1 99–113
www.jcb.org/cgi/doi/10.1083/jcb.201502025

Published June 29, 2015

cytoplasmic face of the SPB, at nuclear membrane–associated interphase MTOCs, and onto preexisting MTs, thus allowing the nucleation of new MTs (Venkatram et al., 2004, 2005; Janson et al., 2005; Samejima et al., 2005, 2010; Zimmerman and Chang, 2005; Lynch et al., 2014). In the latter case, the newly nucleated MT is pulled toward the minus end of the underneath MT template via the motor activity of the kinesin-14 Klp2, until Ase1, a homodimeric MT bundling protein, acts as a brake (Carazo-Salas et al., 2005; Carazo-Salas and Nurse, 2007; Janson et al., 2007; Braun et al., 2009, 2011). The MT length is regulated by several MT plus end tracking proteins including Mal3 (the EB1 homologue) and Tip1 (the Clip170 homologue), two proteins that favor MT rescue (Beinhauer et al., 1997; Brunner and Nurse, 2000; Busch and Brunner, 2004; Höög et al., 2013), Alp14 (a TOG orthologue) that has a MT polymerase activity (Al-Bassam et al., 2012), and the kinesins-8 Klp5 and Klp6 that promote catastrophe (Unsworth et al., 2008; Tischer et al., 2009; Erent et al., 2012). This complex interplay between diverse MAPs results in a typical interphase MT bundle organization, such as within the bundle the overlapping stable MT minus ends are found near the nucleus whereas the dynamic plus ends are extending toward the cell tips (see model in Fig. 8 A; Drummond and Cross, 2000; Piel and Tran, 2009; Hachet et al., 2012). This dynamic arrangement enables the MT plus ends to produce a balance of pushing forces that position the nucleus at the center of the cell (Tran et al., 2001) and will ultimately lead to a symmetrical cell division (Daga and Chang, 2005).

Interphase MT bundles have an additional physiological function. Just after division, cells initiate growth at the preexisting cell end, the old end. Dynamic interphase MTs play an active role in this process. Indeed, by touching the cell cortex, growing MT plus ends deliver polarity factors to cell extremity. One of these factors, the Kelch repeat–containing protein Tea1, docks onto its membrane-associated receptor, the prenylated protein Mod5 (Snaith and Sawin, 2003). Once at the cell tip, Tea1 recruits the Formin For3 and its associated partners, such as Bud6, enabling the nucleation of actin filaments that will be subsequently assembled into actin cables. Actin cables will then serve as tracks for the myosin V–dependent polarized transport of all the building blocks required for cell growth. Hence, in interphase, MTs establish the site of polarized growth and mutations that impinge on interphase MT bundle organization or dynamics consequently affect cell shape (Chang and Martin, 2009; Martin, 2009; Hachet et al., 2012).

Like other eukaryotes, upon nutrient exhaustion, *S. pombe* cells stop growth and proliferation and enter a temporary non-dividing state called quiescence (Sajiki et al., 2009). While quiescence may encompass very different physiological situations depending on the nature of the exhausted nutrient (Costello et al., 1986), it is clear that fission yeast quiescence establishment is accompanied by profound modifications of the cell transcriptome, proteome (Marguerat et al., 2012), and metabolome (Sajiki et al., 2013) and by the acquisition of a variety of features including an enhanced resistance to harmful external conditions or the accumulation of storage molecules (Wei et al., 1993; Su et al., 1996). We have previously shown that upon carbon source exhaustion, the fission yeast proteasome exits the nucleus and forms a specific cytoplasmic structure called proteasome storage granule (Laporte et al., 2008). Such relocalization has also been reported in budding yeast (Laporte et al., 2008). In addition, in *Saccharomyces cerevisiae*, actin filaments collapse into actin bodies (Sagot et al., 2006), and various chaperones (Tapia and Morano, 2010; Liu et al., 2012), enzymes (Narayanaswamy et al., 2009; Noree et al., 2010), or kinases (Shah et al., 2014) are relocalized upon quiescence entry. Some of these reorganizations have been observed in metazoans (Noree et al., 2010), suggesting that they may be conserved among eukaryotes.

In this study, we show that fission yeast cytoskeletons are completely reorganized upon quiescence entry. Indeed, we primarily observed that the MT cytoskeleton is drastically reshaped as quiescent cells assemble a large SPB-associated MT bundle composed of astonishingly stable antiparallel MTs. Importantly, we also report that quiescence establishment comes along with a massive rearrangement of the actin cytoskeleton and the loss of cell polarity. We finally demonstrate that quiescent cell MT elongation is strictly required for cell polarity reestablishment upon quiescence exit.

Results

Upon quiescence entry, *S. pombe* reorganizes its MT cytoskeleton as a single bundle linked to the SPB

Upon carbon source exhaustion, fission yeast cells leave the cell cycle and enter quiescence from interphase (Bostock, 1970; Costello et al., 1986). In these conditions, we have analyzed MT organization in wild-type (WT) cells expressing the α-tubulin 2 (Atb2) fused to GFP. As expected, proliferating interphase cells displayed two to five long cytoplasmic bundles composed of 4 ± 1 MTs (Fig. 1, A and B; Höög et al., 2007). Strikingly, we observed that after carbon exhaustion, the number of MT bundles progressively decreased (Fig. 1 A). Four days after carbon exhaustion, the majority of the cells displayed a single MT bundle (Fig. 1 A and Fig. S1 A) that we named Q-MT bundle, standing for quiescent cell MT bundle. This unique MT bundle was composed of more than 15 MTs (Fig. 1 B) that were not necessarily of the same length, as exemplified by the arrow shape of the bundle extremities (Fig. S1 B). In fact, in ∼15% of the cells, the Q-MT bundle could display internal thickness variations (Fig. S1 C). Importantly, by imaging cells coexpressing GFP-Atb2 with the SPB-associated protein Sfi1 fused to CFP and the nuclear membrane protein Cut11 fused to RFP, we observed that the Q-MT bundle was generally associated with the SPB (>70% of the cells; Fig. 1, C, D, and G), even when quiescence was prolonged (Fig. S1 D). Yet, MT bundles not associated with the SPB displayed the same length and intensity than the SBP-associated ones (Fig. S1, E and F). EM analysis of quiescent WT cells showed that within the Q-MT bundle MTs were regularly spaced (Fig. 1, D–G; and Fig. S1 G). Finally, the Q-MT bundle organization and localization within the cell were confirmed by 3D models constructed using serial section electron tomograms (Fig. 1 G).

The Q-MT bundle is composed of stable MTs

In interphase cells, cytoplasmic MTs are known to be extremely dynamic as they rapidly alternate periods of growth and shrinkage (Fig. 2 A; Drummond and Cross, 2000). They are therefore very sensitive to drugs that inhibit MT polymerization and cause dynamic MT disassembly, such as methyl benzimidazol-2-yl-carbamate (MBC) or thiabendazole (TBZ; Fig. 2 B; Sawin and Nurse, 1998; Sawin and Snaith, 2004). In contrast, we showed that in quiescent cells, the Q-MT bundle had a constant

Published June 29, 2015

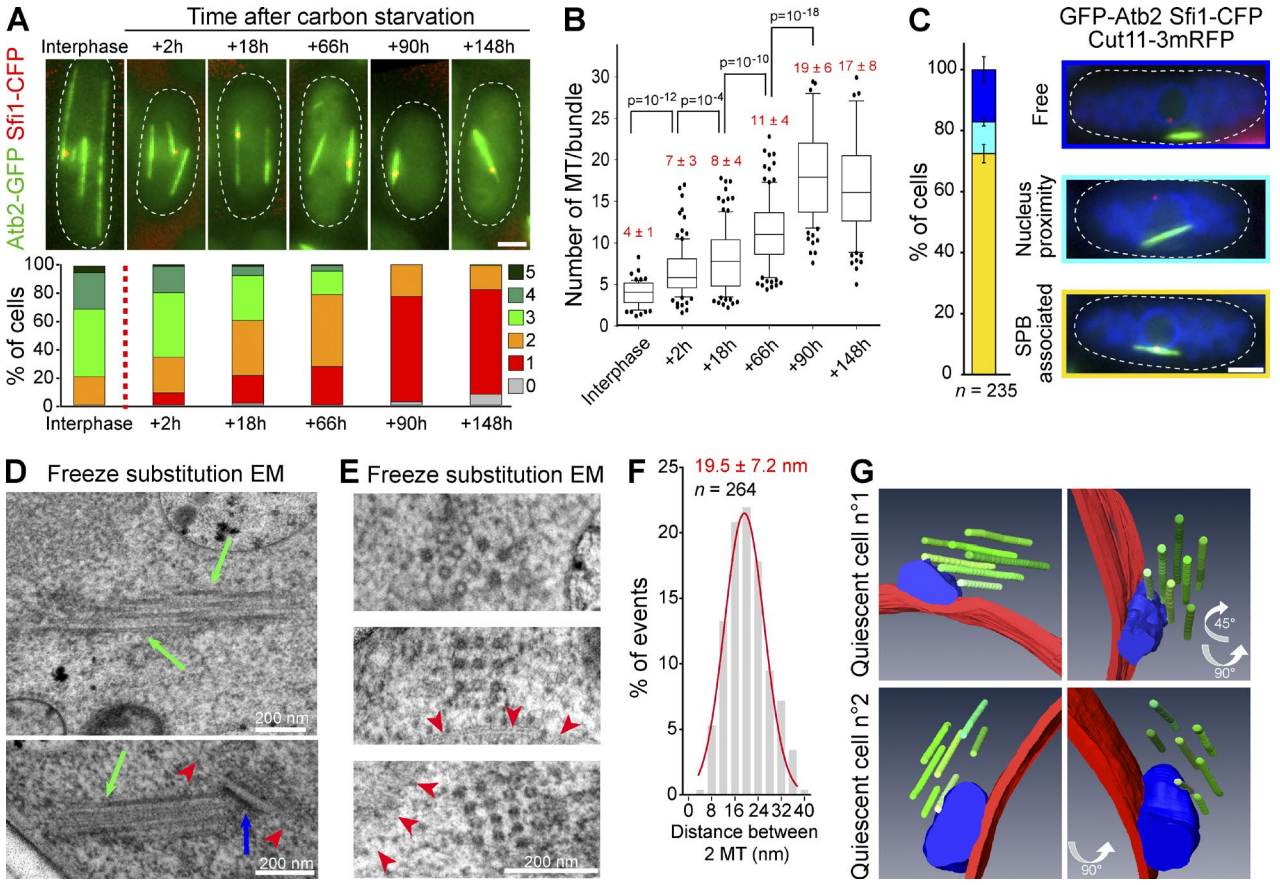

Figure 1. **In quiescence, *S. pombe* assemble a unique MT bundle associated with the SPB.** (A) Cells expressing GFP-Atb2 (green) and Sfi1-CFP (red) are shown (top). The variation of the number of MT bundles per cell is presented as a function of time (bottom; glucose exhaustion is marked by a red dashed line; $n > 200$ cells per time point). (B) The number of MTs per bundle increases upon quiescence entry (p-values are indicated; $n > 100$ cells per time point). (C) The Q-MT bundle is associated with the SPB (N = 2 experiments and $n > 100$ cells). Examples of quiescent cells (5 d) expressing GFP-Atb2 (green), Sfi1-CFP (red), and Cut11-RFP (blue). Bars, 2 µm. (D and E) The Q-MT bundle visualized longitudinally (D) and transversally (E) by freeze substitution EM in WT cells (7 d). Green arrows point at MTs, red arrowheads point at the nuclear membrane, and a blue arrow indicates the SPB. (F) Distance distribution between two MTs measured using images in E. (G) Using serial section electron tomograms, 3D models of Q-MT bundles were designed. MTs are in green, the nuclear membrane is in red, and the SPB is in blue. Two cells are shown using different view angles.

length (Fig. 2 A) and resisted against massive amounts of drugs (Fig. 2 B) or a cold treatment known to cause the disassembly of dynamic MTs (Fig. S2, A and B). Importantly, no fluorescence was recovered after GFP-Atb2 photobleaching, demonstrating that within the Q-MT bundle, not only MTs were stable but also there was no MT sliding (Fig. 2 C). Of note, like cells entering quiescence upon carbon source exhaustion, upon nitrogen starvation, cells also stabilized a unique MT bundle (Fig. S2 C).

MT stabilization is not primarily caused by GTP depletion but rather involves the SPB

Tubulin binds GTP and can hydrolyze this nucleotide. The influence of the tubulin nucleotide status on MT dynamics in vivo is still a mater of debate (Kueh and Mitchison, 2009). We have analyzed the GTP concentration variation upon entry into quiescence after carbon exhaustion using high pressure ionic chromatography and observed a drastic decrease of the intracellular pool of this nucleotide (Fig. 3 A). Mycophenolic acid (MPA) is a drug that specifically inhibits inosine-5′-monophosphate dehydrogenase, the enzyme that catalyzes the conversion of inosine-5′-monophosphate into guanosine-5′-monophosphate (Allison and Eugui, 2000), the GTP precursor. As in other organisms (Qiu et al., 2000), MPA treatment of proliferating *S. pombe* cells caused GTP depletion (Fig. 3 B). The GTP drop was reversed by addition of guanine in the medium, demonstrating the specificity of MPA treatment (Escobar-Henriques et al., 2001). Interestingly, MPA treatment did not significantly affect MT growth or shrinkage rates (Fig. 3 C) nor the MT catastrophe and rescue frequencies (not depicted), excluding the possibility that MT stabilization would be an immediate consequence of GTP depletion upon quiescence entry.

Kinetic analysis of MT stabilization upon entry into quiescence after carbon exhaustion revealed that as early as 6 h after glucose depletion the MT bundle linked to the SPB was more stable, i.e., resistant to the MT-destabilizing drug benomyl, than other MT bundles present in the cell (Fig. 3 D). The stabilization of the SPB-associated MT bundle fit with a non-random stabilization prediction for both early (Fig. 3 E) and late quiescence time points (Fig. S2 D). Collectively, these results indicated that the SPB, rather than the GTP intracellular concentration, played a major role in MT stabilization in quiescence.

A variety of MAPs colocalizes with the Q-MT bundle and influences its length or thickness

To get insights into the mechanism of Q-MT bundle formation, we looked for MAPs colocalizing with this structure. First, we found that astonishingly, in quiescent cells, Mto1 and Mto2

Published June 29, 2015

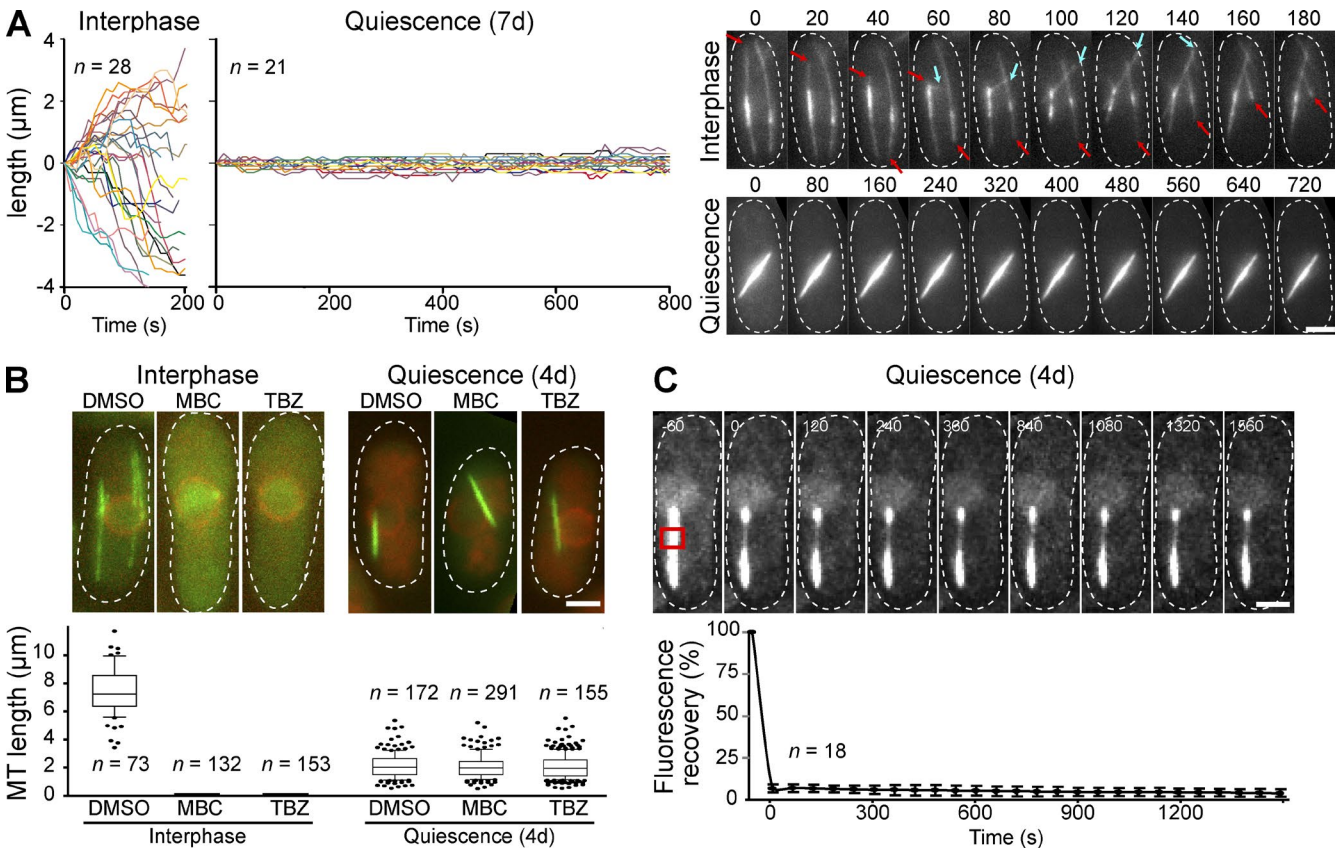

Figure 2. **The Q-MT bundle is composed of stable MTs.** (A) Q-MT bundles do not display detectable length variation. Variation of MT bundle length as a function of time in interphase and quiescent cells. Representative time-lapse movies are shown. Red and blue arrows point, respectively, at shrinking and growing MTs. (B) Q-MT bundles are insensitive to treatments that destabilize dynamic MTs. The graph displays MT bundle length measured in interphase and in quiescent cells (4 d) incubated 30 min with the indicated drugs. Representative cells are shown. (C) FRAP of GFP-Atb2 within a Q-MT bundle measured in quiescent cells (4 d). Error bars are SEM. Time is in seconds. The red box indicates the photobleached area. In all panels, cells are WT cells expressing GFP-Atb2, Sfi1-CFP, and Cut11-RFP. In A and C, only the GFP channel is shown, and in B GFP-Atb2 is in green and Cut11-RFP is in red. Bars, 2 µm.

were no longer found as dots around the nuclear envelope but rather localized exclusively onto the Q-MT bundle (Fig. 4 A and Fig. S3 A). Line scan analyses revealed that Mto1/2 localized as dots that most likely mark the MT ends (Fig. 4 B and Fig. S3 A), in agreement with Mto1/2 being a MT minus end binding complex (Sawin et al., 2004; Venkatram et al., 2004, 2005; Samejima et al., 2005; Janson et al., 2007). Second, the regular spacing between MTs within the Q-MT bundle observed by EM (Fig. 1 E) strongly suggested the presence of a MT bundling protein, and, accordingly, we found that Ase1 localized all along the Q-MT bundle (Fig. 4 C). In *S. pombe*, the CLASP family member Cls1 (Peg1) has been involved in MT stabilization and is known to localize to the overlapping zone of interphase MT bundle (Bratman and Chang, 2007). Similarly, in quiescent cells, we found that Cls1 localized with the denser region of the Q-MT bundle (Fig. 4 C). Finally, the MT plus end tracking proteins Alp7 (the TACC protein orthologue) and Alp14 and Dis1 (two TOG-related proteins) localized as dots that probably correspond to MT extremities within the Q-MT bundle (Fig. 4 C), just like the MT minus end–directed kinesin-14 Klp2, although fewer and fainter Klp2 dots were detected (Fig. 4 C). Of note, Mal3, the EB1 homologue, could not be detected in quiescent cells (unpublished data).

We then analyzed the effect of MAP encoding gene deletion on the Q-MT bundle shape, stability, and formation. None of the deletions tested resulted in the absence of MT bundle (Fig. 4 D) or its destabilization (Fig. S3 C). However, in some mutants, whereas the steady-state level of total α-tubulin remained constant (Fig. S3 B), the Q-MT bundle was either both thicker and longer (*klp5Δklp6Δ*, *alp7Δ*, and *dis1Δ*), just thinner (*ase1Δ*), or both shorter and thinner (*mal3Δ* and *alp14Δ*; Fig. 4, E and F). These results indicated that MAPs involved in interphase MT length regulation are also involved in shaping the Q-MT bundle in quiescence. Besides, mutants with an altered Q-MT shape did not display mortality in quiescence (Fig. S3 D) nor a cell shape defect upon quiescence exit (Fig. S3 E), with the exception of *alp14Δ* cells (see the following paragraph and Fig. 7 C).

The Q-MT bundle rapidly elongates upon quiescence exit

In our experimental conditions, glucose exhaustion is responsible for cell entry into quiescence (Fig. S4 A). When quiescent cells were refed with rich medium, the Q-MT bundle rapidly elongated from both extremities, a proof of the MT antiparallel arrangement within the Q-MT bundle (Fig. 5 A and Fig. S4, B and C). In ∼5 min, dynamic MTs polymerizing from the Q-MT bundle touched the cell poles. Of note, tracking SPB movement upon quiescence exit clearly demonstrated that the Q-MT bundle was attached to the SPB (Fig. S4 E). The MT plus end–tracking protein Alp14, although immobile onto the Q-MT bundle in quiescence (Fig. S4 F), was found at the tip of elongating MTs upon quiescence exit (Figs. 5 B and S4 F). In con-

Published June 29, 2015

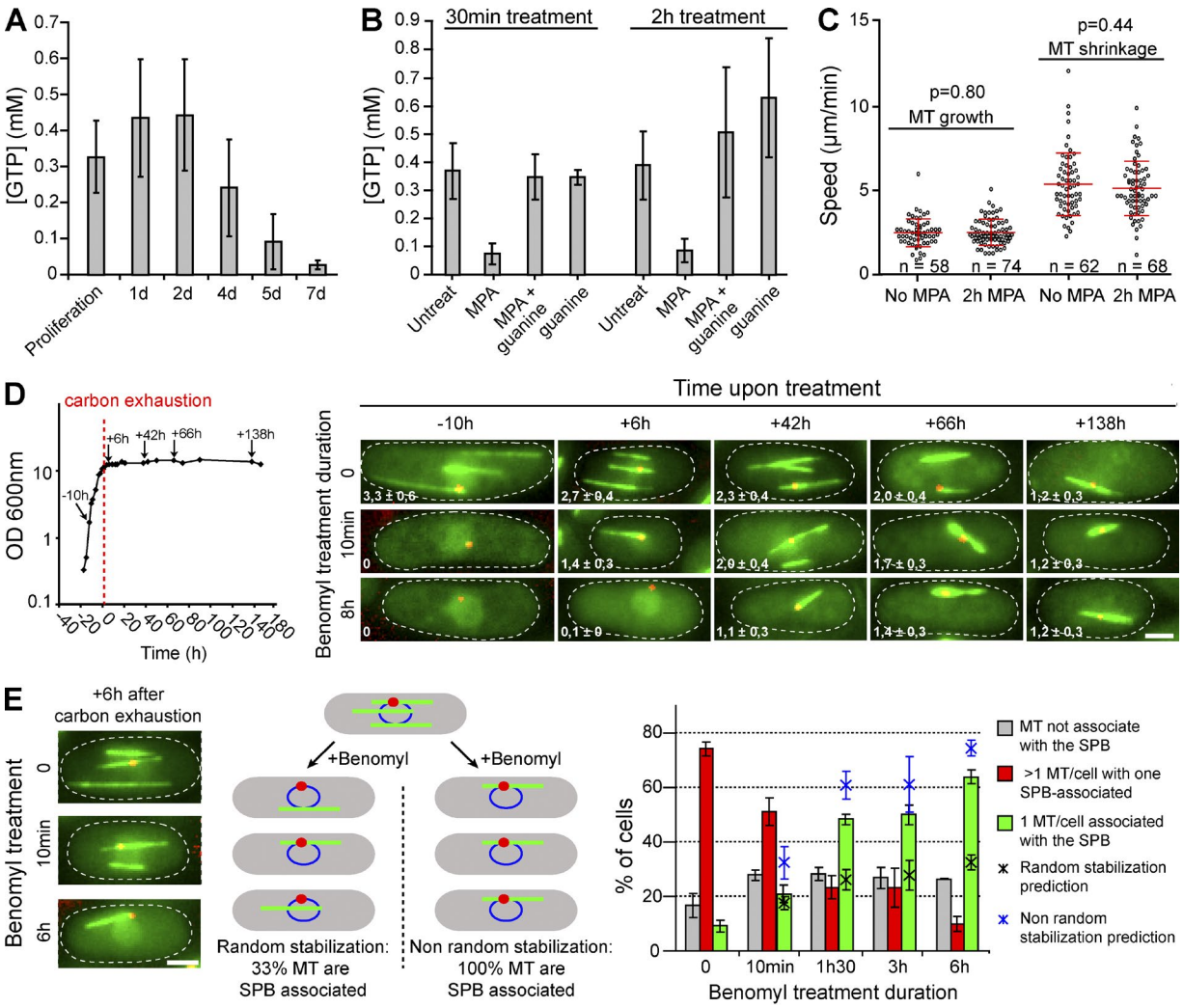

Figure 3. **Q-MT bundle formation does not depend on GTP depletion but rather involves the SPB.** (A) GTP concentration decreases upon quiescence entry. (B) In proliferating cells, a MPA treatment (100 µg/ml) causes a massive GTP concentration drop. Proliferating cells were incubated 30 min or 2 h with either MPA, MPA + guanine (0.3 mM) to reverse the MPA effect, or guanine alone as a control. In A and B, N = 4 experiments with two samples per experiment. (C) MPA-induced GTP droop does not affect MT dynamics in proliferating cells. MT growth and shrinkage speed were determined in proliferating WT cells expressing GFP-Atb2 treated (2 h) or not with MPA. (D and E) MT stabilization involves the SPB. (D) At various times after carbon exhaustion (left, red dashed line), cell expressing GFP-Atb2 (green) and Sfi1-CFP (red) were treated for 10 min or 8 h with benomyl and then imaged. Numbers indicate the mean number of MT bundle per cell (N = 2 experiments and *n* > 200 cells for each time point). (E) WT cells were grown 6 h after carbon starvation and incubated with benomyl for the indicated times (left). A cartoon (middle) representing either a MT bundle random stabilization model or model biased toward the stabilization of the SPB-associated MT bundle. Red, SPB; blue, nuclear membrane; green, MT bundle. Cells displaying multiple MT bundles (red bars) or only a single MT bundle associated with the SPB (green bars) or not (gray bars) were scored for cells incubated with benomyl for the indicated times. N = 3 experiments and *n* > 200 cells per time point. Error bars are SD. The percentage of cells displaying a unique MT bundle associated with the SPB calculated theoretically using a random stabilization prediction (black asterisks) or SPB-biased stabilization (blue askterisks) are indicated (see Materials and methods for details). For all graphs, means and SD are indicated. Bars, 2 µm.

trast, the minus end–associated protein Mto2 stayed immobile on the elongating Q-MT bundle (Fig. S4 G). Later (>15 min), new MT bundles were assembled de novo at the nuclear periphery. Interestingly, as for other quiescent cell-specific structures (Laporte et al., 2011, 2013), the sole addition of glucose onto quiescent cells trigged both Q-MT bundle elongation and assembly of new interphase MT bundles at the nuclear periphery (Fig. 5 A). Importantly, these two MT rearrangements occurred even if de novo protein synthesis was inhibited by cycloheximide (CHX; Fig. 5 A). Yet, as expected, cells treated with CHX did not elongate upon refeeding (Fig. S4 D). This experiment demonstrated that the MT cytoskeleton remodeling upon quiescence exit did not need de novo tubulin synthesis.

We then wonder whether, upon quiescence exit, Q-MT bundle elongation was caused by the polymerization of free cytoplasmic tubulin or if it required the depolymerization of the MTs embedded into the Q-MT bundle. Cell treatment with both CHX and TBZ revealed that within the first 30 min after cell refeeding neither the fluorescence nor the length of the quiescent cell Q-MT bundle was affected (Fig. 5 C), indicating that within this time frame the Q-MT bundle did not depolymerized. This was confirmed by the absence of variation of the Q-MT bundle fluorescence intensity for at least 20 min after cell refeeding in the presence of CHX alone (Fig. S4 H). Obviously, a TBZ treatment prevented de novo interphase MT bundle formation at the nuclear membrane. As a control, we showed that inhibiting MT

Published June 29, 2015

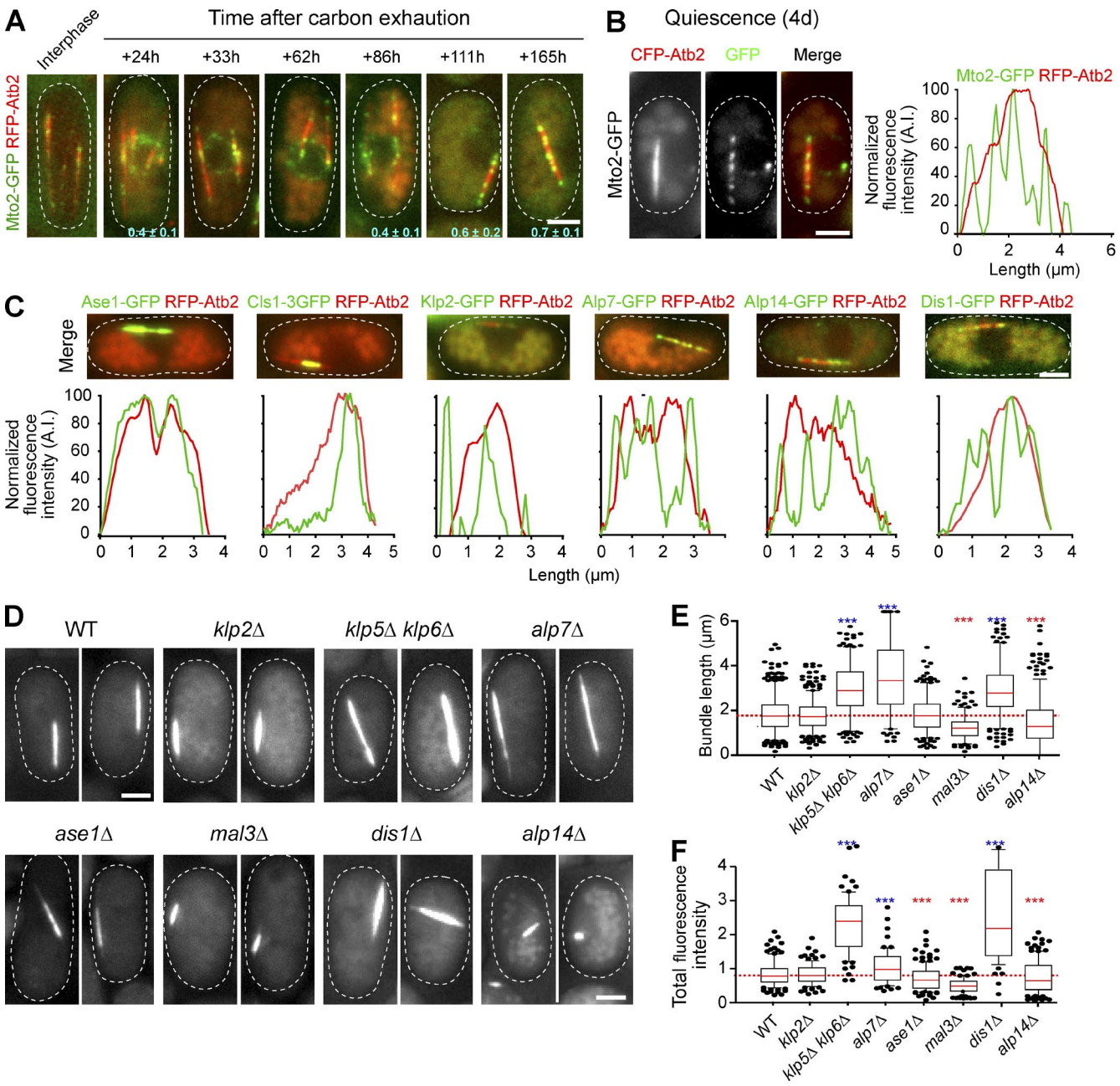

Figure 4. **Various MAPs are associated with the Q-MT bundle and influence its shape.** (A and B) Mto2 relocalizes from the nuclear membrane onto the Q-MT bundle. (A) Cells expressing Mto2-GFP (green) and RFP-Atb2 (red) are shown. Colocalization coefficient between Mto2-GFP and RFP-Atb2 are indicated (see Materials and methods for details). (B) Line-scan analyses (right) indicate that Mto2 localizes at MT extremities within the Q-MT bundle. (C) Numerous MAPs colocalize with the Q-MT bundle. Cells expressing RFP-Atb2 and the indicated MAP fused to GFP were grown 5 d and imaged. Graphs are line scan analyses of the red and green fluorescence. In B and C, data are representative of the fluorescence intensity variations measured out of four experimental repeats. (D–F) The Q-MT bundle shape is influenced by the deletion of specific MAPs. (D) Q-MT bundle was imaged in 7-d-old cells expressing GFP-Atb2 and deleted for the indicated MAP. (E and F) Q-MT bundle length ($n > 200$; E) and Q-MT bundle intensity ($n > 100$; F) were measured in the indicated mutants. ***, $P < 10^{-4}$. Blue and red asterisks shows positive and negative difference, respectively. Bars, 2 µm.

polymerization upon quiescence exit did not influence Q-MT bundle stability. Indeed when quiescent cells were refed with new medium in the presence of CHX, and afterward incubated 10 min with MBC (Fig. S4 I), Q-MT bundle length and fluorescence intensity stayed constant for at least 20 min, whereas MT dynamic was clearly recovered. In fact, Q-MT bundles start to disassemble only 1 h after cells refeeding (Fig. S4 I). Collectively these data demonstrated that a free tubulin pool was present in quiescent cell cytoplasm and that MT elongation upon quiescence exit was caused by free tubulin polymerization at the Q-MT bundle extremities.

S. pombe cells lose their polarity and assemble actin bodies in quiescence

In actively dividing *S.pombe*, MTs deposit polarity factors, such as Tea1, to the cell tip to allow polarized growth (Chang and Martin, 2009; Martin, 2009; Piel and Tran, 2009; Hachet et al., 2012). In quiescent *S. pombe* cells, Tea1 was no longer detected

Published June 29, 2015

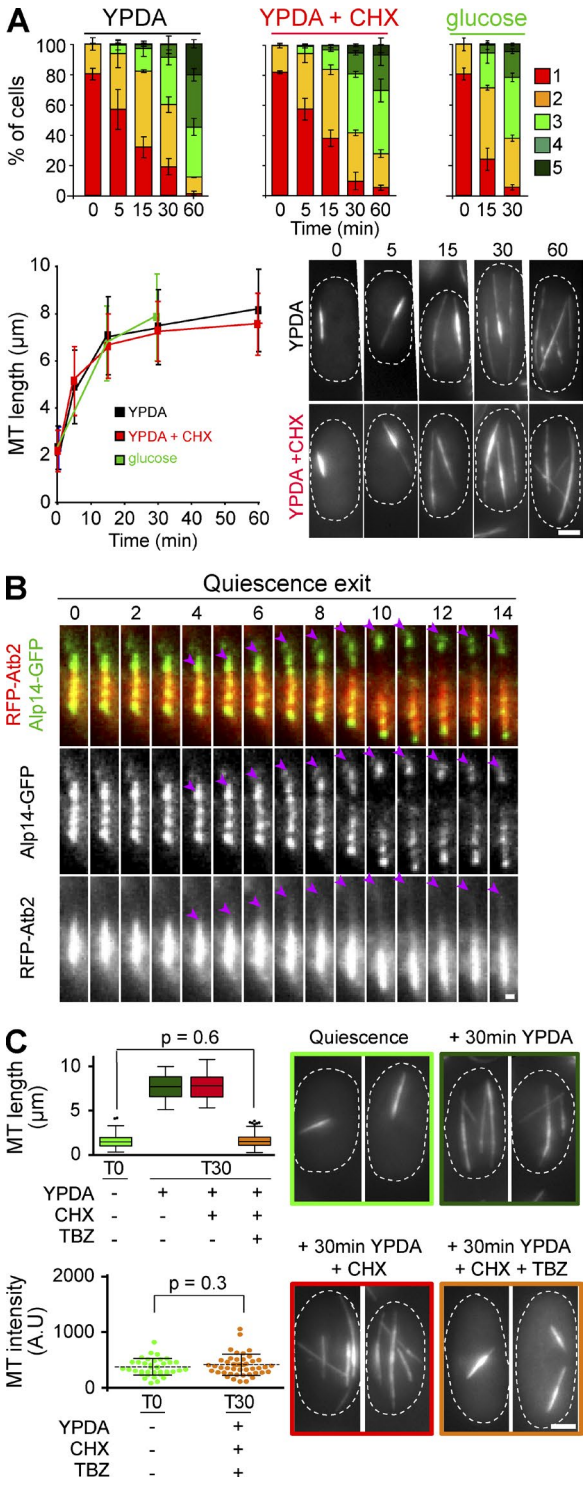

Figure 5. **The Q-MT bundle rapidly elongates upon quiescence exit.** (A) MT cytoskeleton organization before and upon quiescence exit. Quiescent cells (7 d) were refed with YPDA ± CHX or with water containing 2% glucose. The number of MT bundles per cell (top) and the length of the MT bundles (bottom) were then measured (N = 2 experiments and $n > 200$). Representative cells expressing GFP-Atb2 are shown. Means and SDs are indicated. (B) Time-lapse movies of cell coexpressing RFP-Atb2 and Alp14-GFP upon quiescence exit. Alp14 dots (pink arrowhead) follow MT growing tips. Quiescent cells (5 d) were refed with YPDA. The time after cell refeeding is indicated in minutes. (C) The Q-MT bundle stays stable upon quiescence exit. Quiescent cells (7 d) were incubated 30 min in YPDA ± CHX ± TBZ. MT bundle length (top) and fluorescence intensity (bottom) were measured; p-values are indicated. Representative cells are shown. Bars: (A and C) 2 µm; (B) 0.5 µm.

at the cell tips but was rather localized onto the Q-MT bundle (Fig. 6 A). Tip1, a MT plus end tracking protein of the CLIP170 family, was also lost from cell extremities but couldn't be detected in quiescent cells (Fig. 6 A). We made a similar observation for active Cdc42 (CRIB domain), the exocyst components Exo70 and Sec8 (Fig. 6 B), the myosin V myo52, the polarity factor Pob1 (Fig. S5 A), and the formin For3 (not depicted). Interestingly, in quiescent *S. pombe*, no actin cable or patch were found. Instead, we observed a big cytoplasmic F-actin–containing structure (Fig. 6 C). This structure displayed all the characteristics described for actin bodies in quiescent *S. cerevisiae* (Sagot et al., 2006): they do not have a particular size or shape (Fig. 6 C), they are resistant to Latrunculin A (not depicted), and they contain a specific set of actin binding proteins such as fimbrin (Fim1; Fig. 6 C), capping protein (Acp2; Fig. 6 C), and drebrin (Aap1; Fig. S5 A), but not Bud6, Vrp1, Crn1, Arp5, or End4 (Fig. S5 A). These observations indicated that upon glucose exhaustion–induced quiescence entry, *S. pombe* cells lose their polarity and entirely reorganize their actin cytoskeleton.

Q-MT bundle elongation is required for polarity reestablishment upon quiescence exit

Upon quiescence exit, we found that cells rapidly repolarized. Indeed, within minutes, Tea1 returned to the cell tips (Fig. 7 A) as did Tip1 and Pob1 (Fig. S5 B). In parallel, actin bodies quickly disassembled and actin patches reassembled at the cells extremities (Fig. 7 A, Fim1, Acp2, and App1; and Fig. S5 B, Bud6). Of note, Tea1 repolarization could occur even if de novo protein synthesis was inhibited (Fig. S5 C) but, as expected, it was impaired in a *mod5Δ* mutant (Snaith and Sawin, 2003; Fig. S5 D).

To decipher the potential role of the Q-MT bundle in cell repolarization upon quiescence exit, cells exiting quiescence were treated with MBC, a drug that prevents MT bundle elongation and de novo interphase MT bundle formation at the nuclear periphery (Figs. 5 C and S5 C). In these conditions, we found that repolarization of Tea1 and the actin components Fim1, Acp2, and App1 was impaired in >60% of the cells and drastically delayed in the remaining 40% (Fig. 7 A). At later time points, these polarity defects translated into major cell shape defects (Fig. 7 B) that were not observed in the control experiments done with proliferating cells. This strongly suggested that Q-MT bundle elongation and the return to dynamic MT was required for polarity reestablishment upon quiescence exit.

Interestingly, we found that quiescent *alp14Δ* cells were incapable of Q-MT elongation and interphase bundle reassembly upon refeeding (Fig. 7, C and D). This later defect was not the result of an impaired relocalization of Mto1/2 onto the nuclear membrane (Fig. S5 E). This demonstrated that Alp14 was required for Q-MT bundle elongation. Further, as MBC treated cells, *alp14Δ* cells displayed a strong cell shape defect upon quiescence exit (Fig. 7 C), another proof of the involvement of the Q-MT bundle elongation in cell repolarization upon quiescence exit.

To definitively address this point, we used *mto1Δ*, a mutant known to be unable to nucleate cytoplamic MTs (Sawin et al., 2004). Interestingly, after 5 d, *mto1Δ* cells do not assemble a bona fide Q-MT bundle but instead display a unique long and thin MT-containing structure composed of MTs that are sensitive to a cold treatment (Fig. 7, E and F). As *mto1Δ* cells are unable to nucleate cytoplasmic MTs, a shift back to 30°C after a cold treatment did not allow de novo MT polymerization (Fig.

Published June 29, 2015

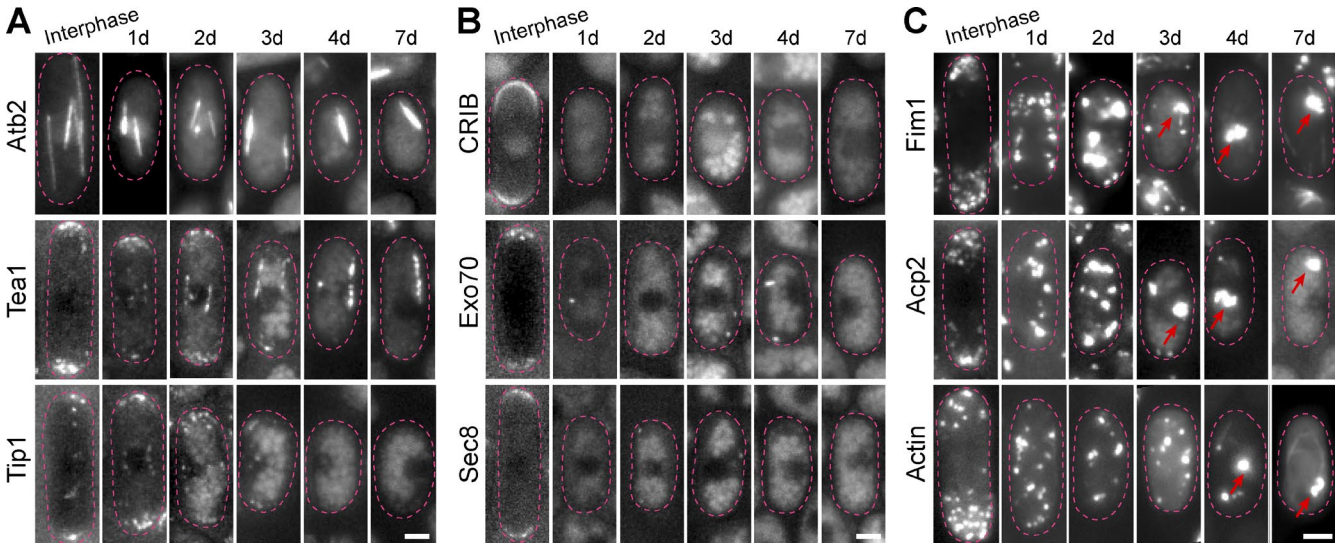

Figure 6. **Quiescent *S. pombe* cells have lost their polarity and reorganized their actin cytoskeleton into actin bodies.** Cells expressing either Atb2-GFP or the polarity markers Tea1-GFP or Tip1-GFP (A), GFP-CRIB or the exocyst component Exo70-GFP or Sec8-GFP (B), or Fim1-GFP or Acp2-GFP (C) are shown upon entry into quiescence. F-actin filaments were detected by Alexa-Phalloidin staining (C, bottom). Red arrows point at actin bodies. Bars, 2 µm.

7 E and not depicted). Using this mutant, we were able to get rid of MTs in quiescence and address the phenotype of cells exiting quiescence in the absence of MTs. As shown in Fig. 7 (E and F), the vast majority of the cold-treated *mto1Δ* cells exiting quiescence without MT exhibit strong polarity and shape defects (see also Fig. S5 F). Collectively, these results demonstrated that the Q-MT bundle elongation and the recovery of dynamic MTs are involved in polarity reestablishment upon quiescence exit.

Discussion

In this study we have shown that when fission yeast cells enter quiescence after carbon source exhaustion, they remodel their MT cytoskeleton into a unique MT bundle (Q-MT bundle). This Q-MT bundle is composed of more than 15 stable and regularly spaced antiparallel MTs. Importantly, this structure is associated with the SPB, a MTOC that seems to be involved in Q-MT bundle MT stabilization (Figs. 1, 2, and 3). We have also observed that the actin cytoskeleton is drastically reshaped as cells disassemble actin patches and cables and assemble actin bodies (Fig. 6), stable F-actin–containing structures (Sagot et al., 2006). In parallel, polarity markers, such as Cdc42, the exocyst components, and Tea1, are lost from cell tips (Fig. 6). All these rearrangements result in a loss of cell polarity in quiescence. When cells exit quiescence, the Q-MT bundle immediately elongates from both extremities and actin bodies dissociate (Figs. 5 and 7). Within an hour, a typical interphase organization is restored, i.e., three to four thin and dynamic MT bundles extend along the long axis of the cell, actin patches and cables assemble at cell tips, and cells start to grow in a polarized manner.

What are the molecular mechanisms involved in Q-MT bundle formation?

Upon quiescence establishment, the SBP-associated MT bundle rapidly becomes more stable compared with other MT bundles present in the cell cytoplasm (Fig. 3 D, t + 6 h). Within <2 d after carbon exhaustion, the SPB-associated MT bundle is fully resistant to treatments that destabilize dynamic MTs. This stabilization will be discussed below. As a second step toward Q-MT bundle formation, we propose that the binding of Mto1/2 onto the SPB-associated MTs allows the nucleation of new MTs (Fig. 8 A, step 2). The displacement of the equilibrium toward de novo MT nucleation by Mto1/2-activated γ-tubulin onto the stable SPB-associated MT bundle may be favored by the concomitant loss of Mto1/2 affinity for the nuclear envelope (Fig. 4 A). As a result, new MTs would pile up onto the SPB-associated MT bundle that progressively thicken, helped by MT bundling activities, including the one of Ase1 (Loïodice et al., 2005; Yamashita et al., 2005) and Clasp (Bratman and Chang, 2007; Fig. 8 A, steps 3 and 4). Interestingly, MAPs that regulate the thickness and the length of interphase MT bundles also influence the Q-MT bundle shape (Fig. 4). Indeed, both in interphase and in quiescence, MT bundles are shorter in a *mal3Δ* mutant (Beinhauer et al., 1997; Fig. 4, D to F) or longer in a *klp5Δklp6Δ* mutant (West et al., 2001; Fig. 4, D to F), in agreement with the molecular activities of these proteins that, respectively, promote MT rescue or catastrophe (Unsworth et al., 2008; Tischer et al., 2009; Erent et al., 2012). Alp14 has a MT polymerase activity in vitro (Al-Bassam et al., 2012) and, accordingly, *alp14Δ* cells display both shorter interphase MT bundles (Al-Bassam et al., 2012) and shorter Q-MT bundles (Fig. 4, D–F). Furthermore, just like interphase MT bundles in proliferating *alp7Δ* cells (Zheng et al., 2006), the Q-MT bundle is longer in quiescent *alp7Δ* cells (Fig. 4, D–F). Finally, consistent with Ase1 bundling activity (Loïodice et al., 2005), we found that the Q-MT bundle is thinner in quiescent *ase1Δ* cells (Fig. 4, D–F). The Q-MT bundle formation may therefore hypothetically rely on a self-assembling mechanisms similar to the one proposed for interphase MT bundles (Carazo-Salas and Nurse, 2006; Daga et al., 2006; Carazo-Salas and Nurse, 2007; Janson et al., 2007; Subramanian and Kapoor, 2012).

How to explain MT stability in quiescence?

During proliferation, nearly 100% of the cells display SPB-associated MTs. In quiescence, ∼75% of the Q-MT bundles are associated with the SPB (Figs. 1 C and S1 D). We have never directly observed a Q-MT bundle "detaching" from the SBP.

Published June 29, 2015

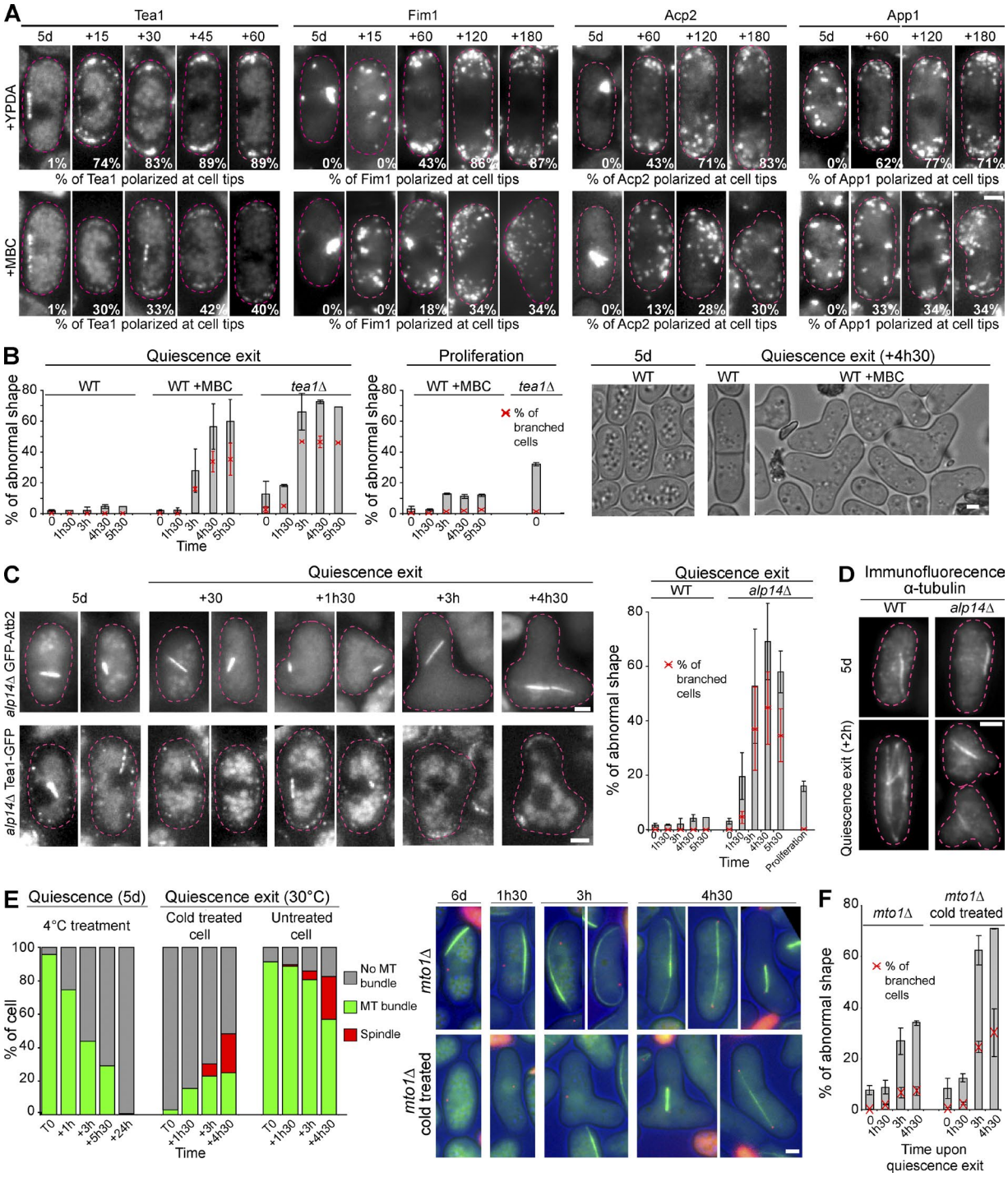

Figure 7. **Q-MT bundle elongation allows cell polarity reestablishment upon quiescence exit.** (A) Quiescence exit of cells expressing the indicated polarity markers was triggered in the absence or presence of MBC. Numbers indicate the percentage of cells with polarized markers at the cell tips (N = 2 experiments and $n > 200$). Time is in minutes. (B–F) Cell shape is drastically impaired when the Q-MT bundle elongation is inhibited. (B) Cell shape was analyzed before and after refeeding of 5-d-old WT cells in the absence or presence of MBC. Control experiments were done in proliferating cells. Representative cells are shown. (C) Upon quiescence exit, the *alp14Δ* mutant is unable to elongate the Q-MT bundle and display massive cell shape defects associated with Tea1-GFP mislocalization. *Alp14Δ* cells expressing either GFP-Atb2 or Tea1-GFP are shown before and after cell refeeding. Cell shape was analyzed before and after refeeding or as a control in proliferation. (D) Control experiment in which tubulin is revealed by immunofluorescence using Tat1 antibodies in both WT and *alp14Δ* mutant cells in quiescence (5 d) and 2 h after quiescence exit. (E) After 5 d in YPD, *mto1Δ*-expressing GFP-Atb2 cells display a long and dynamic MT structure that is destabilized by a cold treatment (4°C for 24 h). When *mto1Δ* cold-treated cells are shifted back to 30°C and then refed, they do not assemble cytoplasmic MT until cells undergo mitosis. Graphs illustrate the number of MT bundles per cell. Data shown are from a single representative experiment out of four repeats (with $n > 200$ for each time point). The corresponding images are shown. (F) Cell shape of cold-treated *mto1Δ* cells was monitored upon quiescence exit. For all graphs, means and SDs are indicated. Bars, 2 µm.

Published June 29, 2015

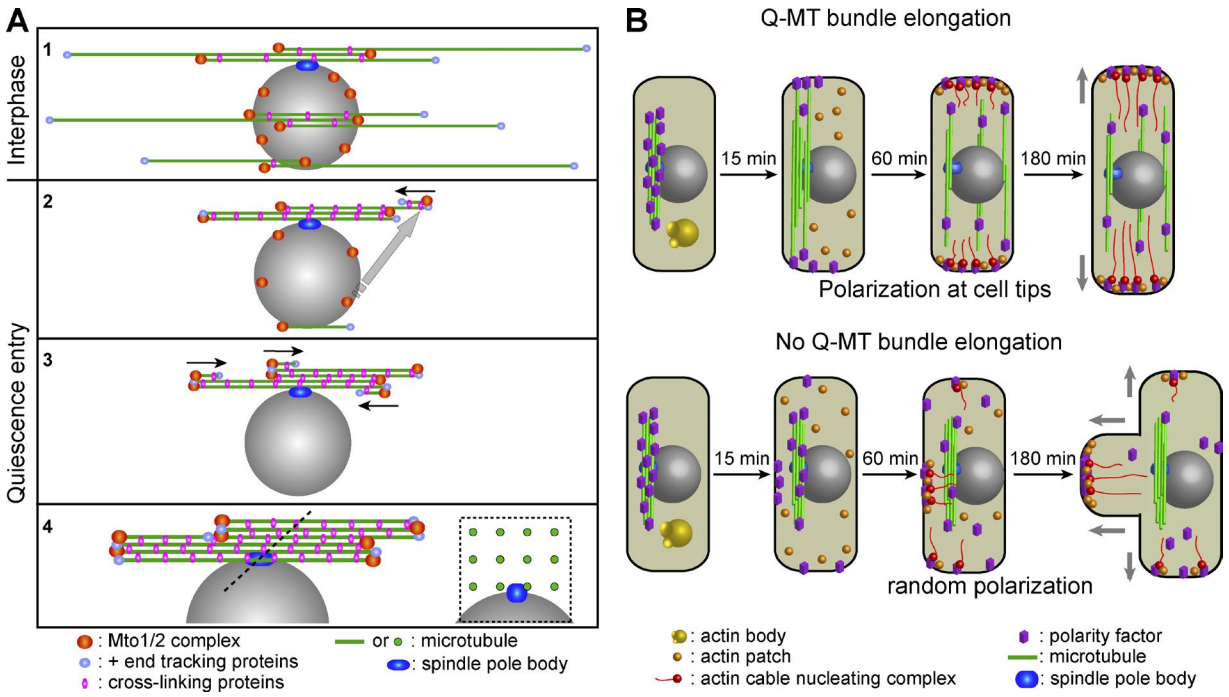

Figure 8. **Schematization of Q-MT bundle assembly and reestablishment of cell polarity upon quiescence exit.** MTs are in green, the nucleus is in gray, and the SPB is in dark blue. (A) The MT minus ends and the Mto1/2 complexes are indicated using orange spheres, the MT plus ends and the associated plus tip tracking proteins are indicated by small light blue spheres, and the bundling proteins are indicated by pink ovals. (B) Polarity factors are in violet, actin bodies are in yellow, actin patches are in orange, and actin cable nucleating complexes containing formins are in red. See Discussion for details.

Therefore, whether free Q-MT bundles result from SPB detachment events or if their stabilization occurred independently of the SPB remain an open question. Yet, whether they are SPB associated or not, Q-MT bundles have an apparent constant length and contain MTs that are insensitive to treatments that destabilize dynamic MTs (Figs. 2, S1 [E and F], and S2 [A and B]).

The molecular events leading to MT stabilization within the Q-MT bundle are still unknown. We can speculate that an enhanced MT cross-linking activity specifically associated with the Q-MT bundle may prevent its depolymerization. Upon quiescence entry, the SPB-associated bundle may recruit proteins that will either modify the bundling activity of known MT cross-linkers, such as Ase1, or load quiescence-specific MT bundling proteins that remain to be identified.

However, an increased MT bundling activity does not explain why MTs apparently do not elongate. We cannot rule out that residual polymerization/depolymerization cycles occur at the MT plus ends. In this scenario, MT elongation would be undetectable using classic fluorescence microscopy because the equilibrium between growth and shrinkage would be displaced toward depolymerization, for example, through the activation of a MT depolymerase. An alternative possibility could be that upon quiescence entry, a MT plus end "capper" would be recruited specifically onto the SPB-associated Q-MT bundle. Although no MT-capping activity has been identified to date, we can envision that a MT plus end tracker, such as a TOG domain–containing protein, for example, could lock MT plus ends, thereby preventing tubulin addition. Finally, the absence of detectable MT elongation in quiescent cells could result from the lack of free polymerizable tubulin. However, we have clearly shown that a free tubulin pool is present in the quiescent cell cytoplasm. Indeed, upon cell refeeding, the Q-MT bundle elongates, even if the de novo protein synthesis is inhibited (Fig. 5, A and C). This elongation occurs without any detectable Q-MT bundle depolymerization (Figs. 5 C and S4, H and I). Could the quiescent cell–free tubulin pool be unable to polymerize? We have shown that quiescence entry is associated with a drastic decrease of the GTP intracellular pool. Yet, an artificial GTP concentration drop does not influence MT dynamic (Fig. 3, A–C), at least within early time points. Further, in vitro experiments have demonstrated that GDP tubulin can polymerize given that few GTP tubulin dimers are present (Valiron et al., 2010). As GTP seems not to be involved, we can speculate that in quiescent cells, free tubulin cannot add on MT ends either because of a posttranslational modification or a tubulin dimer sequestering protein.

Q-MT bundle elongation upon quiescence exit

Whatever the mechanism responsible for the absence of MT dynamics in quiescence, Q-MT bundle elongation is rapidly triggered by glucose upon quiescence exit. This swift event, which does not depend on de novo protein synthesis, probably relies on signaling cascades involving nutrient catabolism (Laporte et al., 2011). Interestingly, we have shown that Q-MT bundle elongation requires Alp14 (Fig. 7, C and D), a protein displaying MT polymerase activity (Al-Bassam et al., 2012). In interphase, Alp14 is not strictly required for MT elongation, probably because its absence is compensated by a protein with a similar activity. In quiescence, this compensating activity may be inhibited or absent. Consequently, Alp14 would be needed for feeding the elongating Q-MT bundle plus ends upon quiescence exit. This is in agreement with the observation that Alp14 stays poised onto the Q-MT bundle plus ends in quiescence and follows MT elongation upon quiescence exit (Fig. 5 B).

Importantly, we have demonstrated that Q-MT bundle elongation and the recovery of MT dynamics is necessary for an

Published June 29, 2015

efficient quiescence exit (Figs. 7 and 8 B). Indeed, cells in which the Q-MT bundle elongation is inhibited either pharmacologically or by the deletion of Alp14 exhibit profound cell shape defects. In these cells, polarity markers relocalize to unspecific cortical regions, leading to a random actin repolarization and ultimately to a branched or triangular cell shape (Fig. 8 B). This abnormal cell repolarization upon quiescence exit is a functional proof of the cell polarity loss in quiescence. Further, it explains the long standing observation that mutants impaired for MT dynamic or polarity factors, such as *tea1Δ* mutant, exhibit more T-shaped cells after a starvation period than during proliferation (Browning et al., 2000; Snaith and Sawin, 2003; Sawin and Snaith, 2004; Fig. 7).

Why would cells need to reorganize their cytoskeletons upon quiescence establishment?

We have previously shown that when budding yeast cells enter quiescence after glucose exhaustion, they assemble a stable MT bundle emanating from the SPB (Laporte et al., 2013). Yet, in contrast to the fission yeast cytoplasmic Q-MT bundle, the *S. cerevisiae* stable MT array is nuclear and composed of parallel MTs (Laporte et al., 2013; Laporte and Sagot, 2014). We do not know what the rationales for these structural differences are, and a wide range of speculations based on various physiological differences between these two species can be drawn. It is intriguing that in both yeasts SPB-associated MTs are stabilized. Could the SPB be a platform that integrates nutritional signals and translates them into MT cytoskeleton reorganizations?

All quiescent cells need to preserve their ability to proliferate and must produce a healthy progeny (Coller, 2011; O'Farrell, 2011). For microorganisms competing for an environmental niche, quiescence exit must be efficient to guarantee the prevalence of the species. Upon quiescence entry, we have shown that *S. pombe* and *S. cerevisiae* cells reorganize both their MT and their actin cytoskeletons to form stable structures (Sagot et al., 2006; Laporte et al., 2013; this study). Whether these reorganizations are just a passive consequence or actively participate in the process of quiescence establishment is a critical question (Daignan-Fornier and Sagot, 2011a,b). Actin and tubulin are very abundant proteins required for cell growth and division. The degradation or the damaging of these proteins in quiescence would require their resynthesis to allow proliferation resumption. This step would need a large amount of amino acids and energy and would require some time that may negatively impinge on the swift reentry into the proliferation cycle. Protein damage might to be a major cause of cell death during a long-term nonproliferative state. Might actin and tubulin be better protected from external damages when packed up into stable polymers rather than as free monomers in the cytoplasm? To definitively address the requirement for actin bodies and stable MT-containing bundles for yeast cell survival in quiescence, conditional mutants or experimental procedures to transiently disassemble these structures in quiescence need to be found.

Nevertheless, here, we have uncovered a physiological function for a quiescent cell–specific structure, as we have shown that fission yeast Q-MT bundle elongation is mandatory for an efficient quiescence exit. As such, this structure clearly participates in the fitness of *S. pombe*, a single-celled eukaryote in competition with numerous other species. Moreover, our study sheds light on the conservation of the reorganization and stabilization of both the actin and the MT cytoskeletons upon quiescence establishment in two phylogenetically distant unicellular eukaryote species. One obvious direction for future studies is to address this conservation in multicellular organisms.

Materials and methods

Strains and growth conditions

Table S1 lists the *S. pombe* strains used in this study. Strains were provided by F. Chang (Columbia University College of Physicians and Surgeons, New York, NY), J.P. Javerzat (Centre National de la Recherche Scientifique, Bordeaux, France), P. Nurse (The Francis Crick Institute, London, UK), A. Paoletti (Institut Curie, Paris, France), P. Perez (Universidad de Salamanca, Salamanca, Spain), K. Sawin (University of Edinburgh, Edinburgh, UK), V. Sirotkin (State University of New York Upstate Medical University, Syracuse, NY), T. Toda (London Research Institute, London, UK), P. Tran (Institut Curie, Paris, France), and J.Q Wu (The Ohio State University, Columbus, OH). All tagged genes are under the control of their endogenous promoters. For all experiments, yeast cells were grown in liquid YPDA medium at 30°C as described previously (Laporte et al., 2008) except for Fig. S1 A and Fig. 3 B for which strains were grown in YE5S+A or in synthetic dextrose medium (2% [wt/vol] glucose, 0.17% [wt/vol]) nitrogen base, and 0.5% [wt/vol] ammonium sulfate] with 0.2% (wt/vol) casamino acids (Difco Laboratories) supplemented with tryptophan and uracil (SD casa WU), respectively. For nitrogen starvation (Fig. S2 C), proliferating cells in EMM2 were washed five times with water, and then transferred in EMM2-N medium at the same cell concentration. For cold treatment, cells were shifted at 4°C for the indicated time, and then shifted back to 30°C and imaged. For drug treatments, cells were incubated with 0.5 mg/ml MBC (Sigma-Aldrich), 0.2 mg/ml benomyl (Sigma-Aldrich), 1 mg/ml TBZ (Sigma-Aldrich), or 180 µM CHX (Sigma-Aldrich) for the indicated time. These concentrations are 10 times higher than the one commonly used with proliferating cells. For quiescence exit in the presence of drugs, cells were preincubated 1 h in the presence of the drug before quiescence exit. For quiescence exit in the sole presence of glucose, cells were washed twice with water, inoculated at $OD_{600nm} = 2$ in a solution containing 2% glucose, and incubated at 30°C. Cell viability was addressed after cell incubation for 5 min in a solution containing 0.2% of methylene blue (Sigma-Aldrich) and 2% sodium citrate (Sigma-Aldrich), pH 7. In this study, all experiments were at least duplicated and for each time point, unless specified, >200 cells were scored.

Metabolomics

High pressure ionic chromatography experiments were done as described previously (Hürlimann et al., 2011). In brief, cellular extracts were prepared by an ethanol extraction. Cells were harvested by rapid filtration, immediately dropped into 5 ml ethanol/10 mM Hepes, pH 7.2 (4/1 vol/vol), and incubated at 80°C for 3 min. Samples were evaporated using a rotavapor apparatus. Residues were resuspended in water and insoluble particles were eliminated by centrifugation. Separation of metabolites was performed on a CarboPac PA1 column, linked to a chromatography workstation (ICS3000; Dionex), using a sodium hydroxide/sodium acetate (50–800 mM) gradient. Nucleotide derivatives were detected with a UV diode array detector (Ultimate 3000RS; Dionex). MPA (Sigma-Aldrich) was used at the final concentration of 100 µg/ml. Guanine was used at the final concentration of 0.3 mM in 0.1 M sodium hydroxide.

Cell staining

For immunofluorescence experiments, cells were harvested by rapid filtration and fixed by washing the filter with methanol at −20°C. Cells

Published June 29, 2015

were further processed for immunofluorescence as described previously (Mata and Nurse, 1997). Anti-tubulin staining used the TAT1 monoclonal tissue culture supernatant (gift of K. Gull, Sir William Dunn School of Pathology, Oxford, UK; Woods et al., 1989) at 1:15 followed by Alexa Fluor 488–goat anti–mouse secondary antibody (Molecular Probes) at 1:500.

For actin phalloidin staining, cells were fixed 1 h with freshly made paraformaldehyde (3.8% final [Sigma-Aldrich] in PEM [0.1 M Pipes, 1 mM EGTA, and 1 mM $MgSO_4$, pH 6.9, with 5 N sodium hydroxide]), vortexed every 10 min for 1 h at 70°C, and then centrifuged 5 min at 3,000 rpm. Cells were then washed twice with PEM and resuspended in 1.5 ml PEM + 1% Triton X-100. Proliferating and quiescent cells were incubated for 30 s and 3 min, respectively. Samples were then washed twice in 1.5 ml PEM and resuspended for 24 h at 4°C in PEM containing 1/10 V of Alexa Fluor Phalloidin (Invitrogen). Finally, cells were washed twice, resuspended in a mounting solution containing 70% glycerol and 5 mg/l paraphenylenediamine, and imaged at room temperature as described previously (Sagot et al., 2006).

For MT behavior after cold experiment (Fig. S2 A), samples were fixed 1 min with formaldehyde (3.8% final; Sigma-Aldrich), washed, resuspended in a mounting solution as above, and imaged.

Fluorescence microscopy

Cells were observed in a fully automated inverted microscope (Axiovert 200M; Carl Zeiss) equipped with a stage (MS-2000; Applied Scientific Instrumentation), a 300-W xenon light source (Lambda LS; Sutter Instrument), a 100× 1.4 NA Plan-Apochromat objective, and a five-position filter turret. For GFP imaging, we used a FITC filter (excitation, HQ487/25; emission, HQ535/40; beam splitter, Q505lp). For RFP imaging, we used a Cy3 filter (excitation, HQ535/50; emission, HQ610/75; beam splitter, Q565lp). For CFP imaging, we used a CFP filter (excitation, HQ436/20; emission, HQ480/40; beam splitter, 455dclp). For YFP imaging, we used a YFP filter (excitation, HQ500/20; emission, HQ535/30; beam splitter, Q515lp). All the filters were purchased from Chroma Technology Corp. Images were acquired using a CoolSnap HQ camera (Roper Scientific). The microscope, camera, and shutters (Uniblitz) were controlled by SlideBook software 5.0 (Intelligent Imaging Innovations). Images are, unless specified, 2D maximal projection of Z-stacks performed using a 0.3-µm step. For live cell imaging, 2 µl of the cell culture were spotted onto a glass slide and immediately imaged at room temperature.

For fluorescence intensity measurement (Figs. 1 B, 4 F, S1 F, and S4 I), a line scan (i1) of *n* pixel width (three to eight, depending on the binning acquisitions parameters) containing both GFP signal and background was drawn along MTs using ImageJ software. A line of 2n pixel width at the same location was drawn to calculate the intensity of the surrounding background (i2). The real intensity (ir) was calculated as follow: ib = (i2 × Area i2) − (i1 × Area i1) and ir = i1 − [ib/(Area i2 − Area i)]. To calculate the number of MTs per structure, individual MT fluorescence was determined by three methods: the fluorescence intensity was measured in proliferation cell on either one MT growing or on the nonoverlapping or overlapping region of the spindle, described to contain 11 MTs (Ding et al., 1993). According to these measurements for a single MT, fluorescence intensity measured upon quiescence entry was converted in MT numbers.

To measure MT length (Figs. 4 E and S1 E), positions of the MT-containing structure extremities were followed over time and compared with a fixed point in the cell using MTrackJ plugin (ImageJ). Euclidian distances (D) between two positions over time were calculated as $D = \sqrt{[(x2 - x1)^2 + (y2 - y1)^2]}$. In time-lapse series (Fig. 2 A), the first measured length was set to zero. The same protocol was applied to measure MT dynamics (Fig. 3 C) and SPB movement in quiescence and upon exit (Fig. S4 E). To measure MT dynamics, four z-frames were acquired every 4 s on proliferating cells treated or not with MPA (2 h). After using a rolling average filter (i.e, the MT extremity fix-point length [w] is the mean of w − 1, w, and w + 1 values), the length was plotted over time and growth/shrinkage speed was calculated over a 300-s observation period.

FRAP experiment (Fig. 3 C) was done as previously described (Laporte et al., 2013). Experiments were done on an inverted microscope (DMI 6000; Leica) equipped with a spinning disk confocal head (CSU-X1; Yokogawa Electric Corporation), a QuantEM camera (Photometrics), and a scanner FRAP system (Roper Scientific). The diode lasers used were at 408 and 491 nm. The objective used was an HCX PL APO CS 100× oil with 1.4 NA. The Z-stacks were done with an objective scanner (Piezo P721.LLQ; Physik Instrumente). This system was controlled by MetaMorph software (Molecular Devices). Recovery from photobleaching was monitored in time-lapse mode. Fluorescence recovery was corrected for background noise and continuous photobleaching using the ImageJ software. Fluorescence was then normalized using a rolling average filter (i.e, the fluorescence intensity y is the mean intensity of y − 1, y, and y + 1). The fluorescence was then normalized to the one measured before bleach (Vavylonis et al., 2008).

For line scan analysis (Fig. 4, B and C; and Fig. S3 A), the real measured intensities (ir) were set to percent, with 100% being the maximum calculated along the line. Slopes were manually aligned to zero, with zero being when ir > 0. The same protocol was applied to compare the different slopes after line scan analysis (Fig. S1, B and C).

Mander's colocalization coefficients (Fig. 4 A) were calculated using ImageJ software as described in Jimenez et al. (2014). In brief, Z-stacks were first maximum projected and cells were individually selected in both GFP and RFP channels. The same threshold was applied for each channel and signals were binarized (i.e., pixel < threshold = 0 and pixel > threshold = 255). The percentages of GFP pixel (Mto2-GFP signal) that colocalize with RFP pixel (RFP-Atb2 signal) were determined using the JACoP plugin (Bolte and Cordelières, 2006).

For Q-MT bundle fluorescence measurements upon quiescence exit (Fig. S4 H), a line scan of 8-pixel width was drawn along Q-MT bundle using ImageJ software. The fluorescence intensities were measured in function of time and were corrected for photobleaching. Photobleaching was measured on Q-MT bundles in quiescence images with the same acquisitions conditions.

To calculate the theoretical stabilization of MT upon quiescence entry, we started with the mean number (N) of MT bundles observed for cells before treatment (i.e., for 6 h after carbon exhaustion [Fig. 3 E] the mean number of MT bundle per cell N was 2.7 and for 42 h [Fig. S2 D] N was 3.3). We noted $n_{i\text{-}single}$, the initial percentage of cells with only a single MT bundle. We noted $n_{multi\text{-}before}$ and $n_{multi\text{-}after}$, the percentage of cells with more than one MT bundle observed before and after benomyl treatment, respectively. For each time point, $\Delta_{n\text{-}multi}$ is equal to $n_{multi\text{-}before} - n_{multi\text{-}after}$. For the random stabilization model, we considered that 1/N of the MT bundle is stabilized, regardless of the association with the SPB. Thus, for each time point, the prediction of the percentage of cells that should display a single MT bundle associated for the SPB is $(1/N \times \Delta_{n\text{-}multi}) + n_{i\text{-}single}$. For the nonrandom stabilization, we considered that only the MT bundle associated with the SPB is stabilized. Thus, for each time point, the prediction of the percentage of cells that should display a single MT bundle associated for the SPB is $(\Delta_{n\text{-}multi}) + n_{i\text{-}single}$.

EM

Freezing, freeze substitution (Fig. 1, D and E), and immunostaining (Fig. S1 G) were performed as described previously (Laporte et al., 2013). In brief, cells were washed with glycine, and then with fetal

calf serum, and incubated with polyclonal rabbit anti-Tat1 (the *Trypanosoma brucei* α-tubulin) antibodies diluted 1:250 (a gift of K. Gull; Woods et al., 1989). After a wash with Tris-buffered saline containing 0.1% bovine serum albumin, cells were incubated for 45 min at room temperature with anti–mouse IgG conjugated to 10-nm gold particles (BioCell Laboratories, Inc.). For freeze substitution, yeast were deposited on a copper grid (400 mesh) coated with Formvar. Grids were immersed in liquid propane held at −180°C by liquid nitrogen and then transferred in a 4% osmium tetroxide solution in dry acetone at −82°C for 72 h. Grids were then shifted to room temperature and washed three times with dry acetone. Cell were stained with 1% uranyl acetate and then washed once with dry acetone. Samples were gradually unfiltered with araldite (Fluka). Ultra-thin sections were contrasted with lead citrate and observed in an electron microscope (80 kV; 7650; Hitachi) at the EM facility of the Bordeaux Imaging Center.

For tomography analysis (Fig. 1 G), 150-nm-thick sections were placed on formvar-coated 150-mesh copper grids and poststained 1 min with lead citrate 2% in water. Images were acquired using a Spirit Twin (FEI Tecnai) operated at 120 kV. Images were recorded with a 4k Eagle charge coupled device camera system (FEI Tecnai) at a nominal magnification of 30,000 (sample D7) or 26,000 (sample C10) using a –65 to 65 tilt for Cell 1 or a −65 to 39 for Cell 2 with 2° increments. Tomography tilt series were taken using the batch tomography software (FEI Tecnai). They were then aligned, cropped, and binned using the ETomo program from the IMOD suite. The 3D tomography reconstructed visualization was done using Amira Resolve RT 5.2.0.

For MT distance measurements between two MTs (Fig. 1 F), the centroid of each MT was determined and the Euclidian distance was determined as $D = \{\sqrt{[(x2 - x1)^2 + (y2 - y1)^2]}\}$. This distance was then subtracted for the two MTs' radiuses (~22 nm). Gaussian fit on these values was then determined using GraphPad Prism (GraphPad Software).

Miscellaneous

Glucose concentration was measured using the D-Glucose/D-Fructose UV test kit (Roche). Ade13 polyclonal antibodies were raised in rabbit using the purified full-length *S. cerevisiae* protein (Takara Bio Inc.).

Online supplemental material

Fig. S1 describes the shape of the Q-MT bundle and its detection by EM using immunogold labeling with anti-tubulin antibodies. Fig. S2 analyzes the Q-MT bundle resistance to a cold treatment and its stabilization with time in quiescence after carbon or nitrogen exhaustion. Fig. S3 provides the localization of Mto1-GFP onto the Q-MT bundle. It shows Western blot quantifying the tubulin steady-state amounts, the Q-MT bundle resistance to benomyl, and the viability of MAP mutants in quiescence. Fig. S4 shows MT elongation at Q-MT bundle extremities and Q-MT bundle stability upon quiescence exit. It also shows Q-MT bundle anchoring at the SPB and Alp14-GFP localization during the quiescence exit process. Fig. S5 displays polarity marker localization upon quiescence entry and exit in WT and mutant backgrounds or in the presence of drugs. Table S1 lists the *S. pombe* strains used in this study. Online supplemental material is available at http://www.jcb.org/cgi/content/full/jcb.201502025/DC1.

Acknowledgments

We express our profound gratitude to J.P. Javerzat for precious comments and great discussions about our work and his help in writing this manuscript. We are grateful to M. Gupta, A. Paoletti, D. Pellman, and P. Tran for helpful discussions. We are thankful to F. Chang, J.P. Javerzat, P. Nurse, A. Paoletti, P. Perez, K. Sawin, V. Sirotkin, T. Toda, P. Tran, and J.-Q. Wu for providing yeast strains. We thank A. Lebaudy and M. Revilla Guarinos for their help in preliminary experiments. FRAP was done at the Bordeaux Imaging Center facility with the help of Christel Poujol.

This work was supported by the Université Bordeaux and a Young Investigator grant from the Agence Nationale pour la Recherche (JC08 310804 to I. Sagot).

The authors declare no competing financial interests.

Submitted: 6 February 2015
Accepted: 1 June 2015

References

Al-Bassam, J., H. Kim, I. Flor-Parra, N. Lal, H. Velji, and F. Chang. 2012. Fission yeast Alp14 is a dose-dependent plus end–tracking microtubule polymerase. *Mol. Biol. Cell.* 23:2878–2890. http://dx.doi.org/10.1091/mbc.E12-03-0205

Allison, A.C., and E.M. Eugui. 2000. Mycophenolate mofetil and its mechanisms of action. *Immunopharmacology.* 47:85–118. http://dx.doi.org/10.1016/S0162-3109(00)00188-0

Alushin, G.M., G.C. Lander, E.H. Kellogg, R. Zhang, D. Baker, and E. Nogales. 2014. High-resolution microtubule structures reveal the structural transitions in αβ-tubulin upon GTP hydrolysis. *Cell.* 157:1117–1129. http://dx.doi.org/10.1016/j.cell.2014.03.053

Beinhauer, J.D., I.M. Hagan, J.H. Hegemann, and U. Fleig. 1997. Mal3, the fission yeast homologue of the human APC-interacting protein EB-1 is required for microtubule integrity and the maintenance of cell form. *J. Cell Biol.* 139:717–728. http://dx.doi.org/10.1083/jcb.139.3.717

Bolte, S., and F.P. Cordelières. 2006. A guided tour into subcellular colocalization analysis in light microscopy. *J. Microsc.* 224:213–232. http://dx.doi.org/10.1111/j.1365-2818.2006.01706.x

Bostock, C.J. 1970. DNA synthesis in the fission yeast *Schizosaccharomyces pombe*. *Exp. Cell Res.* 60:16–26. http://dx.doi.org/10.1016/0014-4827(70)90484-2

Bratman, S.V., and F. Chang. 2007. Stabilization of overlapping microtubules by fission yeast CLASP. *Dev. Cell.* 13:812–827. http://dx.doi.org/10.1016/j.devcel.2007.10.015

Braun, M., D.R. Drummond, R.A. Cross, and A.D. McAinsh. 2009. The kinesin-14 Klp2 organizes microtubules into parallel bundles by an ATP-dependent sorting mechanism. *Nat. Cell Biol.* 11:724–730. http://dx.doi.org/10.1038/ncb1878

Braun, M., Z. Lansky, G. Fink, F. Ruhnow, S. Diez, and M.E. Janson. 2011. Adaptive braking by Ase1 prevents overlapping microtubules from sliding completely apart. *Nat. Cell Biol.* 13:1259–1264. http://dx.doi.org/10.1038/ncb2323

Browning, H., J. Hayles, J. Mata, L. Aveline, P. Nurse, and J.R. McIntosh. 2000. Tea2p is a kinesin-like protein required to generate polarized growth in fission yeast. *J. Cell Biol.* 151:15–28. http://dx.doi.org/10.1083/jcb.151.1.15

Brunner, D., and P. Nurse. 2000. CLIP170-like tip1p spatially organizes microtubular dynamics in fission yeast. *Cell.* 102:695–704. http://dx.doi.org/10.1016/S0092-8674(00)00091-X

Busch, K.E., and D. Brunner. 2004. The microtubule plus end-tracking proteins mal3p and tip1p cooperate for cell-end targeting of interphase microtubules. *Curr. Biol.* 14:548–559. http://dx.doi.org/10.1016/j.cub.2004.03.029

Carazo-Salas, R.E., and P. Nurse. 2006. Self-organization of interphase microtubule arrays in fission yeast. *Nat. Cell Biol.* 8:1102–1107. http://dx.doi.org/10.1038/ncb1479

Carazo-Salas, R., and P. Nurse. 2007. Sorting out interphase microtubules. *Mol. Syst. Biol.* 3:95. http://dx.doi.org/10.1038/msb4100136

Carazo-Salas, R.E., C. Antony, and P. Nurse. 2005. The kinesin Klp2 mediates polarization of interphase microtubules in fission yeast. *Science.* 309:297–300. http://dx.doi.org/10.1126/science.1113465

Carlier, M.F., and D. Pantaloni. 1981. Kinetic analysis of guanosine 5′-triphosphate hydrolysis associated with tubulin polymerization. *Biochemistry.* 20:1918–1924. http://dx.doi.org/10.1021/bi00510a030

Chang, F., and S.G. Martin. 2009. Shaping fission yeast with microtubules. *Cold Spring Harb. Perspect. Biol.* 1:a001347. http://dx.doi.org/10.1101/cshperspect.a001347

Coller, H.A. 2011. Cell biology. The essence of quiescence. *Science.* 334:1074–1075. http://dx.doi.org/10.1126/science.1216242

Costello, G., L. Rodgers, and D. Beach. 1986. Fission yeast enters the stationary phase G_0 state from either mitotic G_1 or G_2. *Curr. Genet.* 11:119–125. http://dx.doi.org/10.1007/BF00378203

Daga, R.R., and F. Chang. 2005. Dynamic positioning of the fission yeast cell division plane. *Proc. Natl. Acad. Sci. USA.* 102:8228–8232. http://dx.doi.org/10.1073/pnas.0409021102

Daga, R.R., K.-G. Lee, S. Bratman, S. Salas-Pino, and F. Chang. 2006. Self-organization of microtubule bundles in anucleate fission yeast cells. *Nat. Cell Biol.* 8:1108–1113. http://dx.doi.org/10.1038/ncb1480

Daignan-Fornier, B., and I. Sagot. 2011a. Proliferation/quiescence: When to start? Where to stop? What to stock? *Cell Div.* 6:20. http://dx.doi.org/10.1186/1747-1028-6-20

Daignan-Fornier, B., and I. Sagot. 2011b. Proliferation/quiescence: the controversial "aller-retour." *Cell Div.* 6:10. http://dx.doi.org/10.1186/1747-1028-6-10

Ding, R., K.L. McDonald, and J.R. McIntosh. 1993. Three-dimensional reconstruction and analysis of mitotic spindles from the yeast, *Schizosaccharomyces pombe*. *J. Cell Biol.* 120:141–151. http://dx.doi.org/10.1083/jcb.120.1.141

Drummond, D.R., and R.A. Cross. 2000. Dynamics of interphase microtubules in *Schizosaccharomyces pombe*. *Curr. Biol.* 10:766–775. http://dx.doi.org/10.1016/S0960-9822(00)00570-4

Erent, M., D.R. Drummond, and R.A. Cross. 2012. *S. pombe* kinesins-8 promote both nucleation and catastrophe of microtubules. *PLoS ONE.* 7:e30738. http://dx.doi.org/10.1371/journal.pone.0030738

Escobar-Henriques, M., A. Balguerie, C. Monribot, H. Boucherie, and B. Daignan-Fornier. 2001. Proteome analysis and morphological studies reveal multiple effects of the immunosuppressive drug mycophenolic acid specifically resulting from guanylic nucleotide depletion. *J. Biol. Chem.* 276:46237–46242. http://dx.doi.org/10.1074/jbc.M103416200

Hachet, O., F.O. Bendezú, and S.G. Martin. 2012. Fission yeast: in shape to divide. *Curr. Opin. Cell Biol.* 24:858–864. http://dx.doi.org/10.1016/j.ceb.2012.10.001

Hagan, I.M. 1998. The fission yeast microtubule cytoskeleton. *J. Cell Sci.* 111:1603–1612.

Hagan, I.M., and J. Petersen. 2000. The microtubule organizing centers of *Schizosaccharomyces pombe*. *Curr. Top. Dev. Biol.* 49:133–159.

Höög, J.L., C. Schwartz, A.T. Noon, E.T. O'Toole, D.N. Mastronarde, J.R. McIntosh, and C. Antony. 2007. Organization of interphase microtubules in fission yeast analyzed by electron tomography. *Dev. Cell.* 12:349–361. http://dx.doi.org/10.1016/j.devcel.2007.01.020

Höög, J.L., S.M. Huisman, D. Brunner, and C. Antony. 2013. Electron tomography reveals novel microtubule lattice and microtubule organizing centre defects in +TIP mutants. *PLoS ONE.* 8:e61698. http://dx.doi.org/10.1371/journal.pone.0061698

Horio, T., and T. Murata. 2014. The role of dynamic instability in microtubule organization. *Front. Plant Sci.* 5:511. http://dx.doi.org/10.3389/fpls.2014.00511

Hürlimann, H.C., B. Laloo, B. Simon-Kayser, C. Saint-Marc, F. Coulpier, S. Lemoine, B. Daignan-Fornier, and B. Pinson. 2011. Physiological and toxic effects of purine intermediate 5-amino-4-imidazolecarboxamide ribonucleotide (AICAR) in yeast. *J. Biol. Chem.* 286:30994–31002. http://dx.doi.org/10.1074/jbc.M111.262659

Janson, M.E., T.G. Setty, A. Paoletti, and P.T. Tran. 2005. Efficient formation of bipolar microtubule bundles requires microtubule-bound γ-tubulin complexes. *J. Cell Biol.* 169:297–308. http://dx.doi.org/10.1083/jcb.200410119

Janson, M.E., R. Loughlin, I. Loïodice, C. Fu, D. Brunner, F.J. Nédélec, and P.T. Tran. 2007. Crosslinkers and motors organize dynamic microtubules to form stable bipolar arrays in fission yeast. *Cell.* 128:357–368. http://dx.doi.org/10.1016/j.cell.2006.12.030

Jimenez, L., D. Laporte, S. Duvezin-Caubet, F. Courtout, and I. Sagot. 2014. Mitochondrial ATP synthases cluster as discrete domains that reorganize with the cellular demand for oxidative phosphorylation. *J. Cell Sci.* 127:719–726. http://dx.doi.org/10.1242/jcs.137141

Kollman, J.M., A. Merdes, L. Mourey, and D.A. Agard. 2011. Microtubule nucleation by γ-tubulin complexes. *Nat. Rev. Mol. Cell Biol.* 12:709–721. http://dx.doi.org/10.1038/nrm3209

Kueh, H.Y., and T.J. Mitchison. 2009. Structural plasticity in actin and tubulin polymer dynamics. *Science.* 325:960–963. http://dx.doi.org/10.1126/science.1168823

Laporte, D., and I. Sagot. 2014. Microtubules move the nucleus to quiescence. *Nucleus.* 5:113–118. http://dx.doi.org/10.4161/nucl.28538

Laporte, D., B. Salin, B. Daignan-Fornier, and I. Sagot. 2008. Reversible cytoplasmic localization of the proteasome in quiescent yeast cells. *J. Cell Biol.* 181:737–745. http://dx.doi.org/10.1083/jcb.200711154

Laporte, D., A. Lebaudy, A. Sahin, B. Pinson, J. Ceschin, B. Daignan-Fornier, and I. Sagot. 2011. Metabolic status rather than cell cycle signals control quiescence entry and exit. *J. Cell Biol.* 192:949–957. http://dx.doi.org/10.1083/jcb.201009028

Laporte, D., F. Courtout, B. Salin, J. Ceschin, and I. Sagot. 2013. An array of nuclear microtubules reorganizes the budding yeast nucleus during quiescence. *J. Cell Biol.* 203:585–594. http://dx.doi.org/10.1083/jcb.201306075

Liu, I.-C., S.-W. Chiu, H.-Y. Lee, and J.-Y. Leu. 2012. The histone deacetylase Hos2 forms an Hsp42-dependent cytoplasmic granule in quiescent yeast cells. *Mol. Biol. Cell.* 23:1231–1242. http://dx.doi.org/10.1091/mbc.E11-09-0752

Loïodice, I., J. Staub, T.G. Setty, N.-P.T. Nguyen, A. Paoletti, and P.T. Tran. 2005. Ase1p organizes antiparallel microtubule arrays during interphase and mitosis in fission yeast. *Mol. Biol. Cell.* 16:1756–1768. http://dx.doi.org/10.1091/mbc.E04-10-0899

Lynch, E.M., L.M. Groocock, W.E. Borek, and K.E. Sawin. 2014. Activation of the γ-tubulin complex by the Mto1/2 complex. *Curr. Biol.* 24:896–903. http://dx.doi.org/10.1016/j.cub.2014.03.006

Marguerat, S., A. Schmidt, S. Codlin, W. Chen, R. Aebersold, and J. Bähler. 2012. Quantitative analysis of fission yeast transcriptomes and proteomes in proliferating and quiescent cells. *Cell.* 151:671–683. http://dx.doi.org/10.1016/j.cell.2012.09.019

Martin, S.G. 2009. Microtubule-dependent cell morphogenesis in the fission yeast. *Trends Cell Biol.* 19:447–454. http://dx.doi.org/10.1016/j.tcb.2009.06.003

Mata, J., and P. Nurse. 1997. tea1 and the microtubular cytoskeleton are important for generating global spatial order within the fission yeast cell. *Cell.* 89:939–949. http://dx.doi.org/10.1016/S0092-8674(00)80279-2

Mitchison, T.J. 2014. The engine of microtubule dynamics comes into focus. *Cell.* 157:1008–1010. http://dx.doi.org/10.1016/j.cell.2014.05.001

Mitchison, T., and M. Kirschner. 1984. Dynamic instability of microtubule growth. *Nature.* 312:237–242. http://dx.doi.org/10.1038/312237a0

Narayanaswamy, R., M. Levy, M. Tsechansky, G.M. Stovall, J.D. O'Connell, J. Mirrielees, A.D. Ellington, and E.M. Marcotte. 2009. Widespread reorganization of metabolic enzymes into reversible assemblies upon nutrient starvation. *Proc. Natl. Acad. Sci. USA.* 106:10147–10152. http://dx.doi.org/10.1073/pnas.0812771106

Nogales, E., and H.-W. Wang. 2006. Structural intermediates in microtubule assembly and disassembly: how and why? *Curr. Opin. Cell Biol.* 18:179–184. http://dx.doi.org/10.1016/j.ceb.2006.02.009

Noree, C., B.K. Sato, R.M. Broyer, and J.E. Wilhelm. 2010. Identification of novel filament-forming proteins in *Saccharomyces cerevisiae* and *Drosophila melanogaster*. *J. Cell Biol.* 190:541–551. http://dx.doi.org/10.1083/jcb.201003001

O'Farrell, P.H. 2011. Quiescence: early evolutionary origins and universality do not imply uniformity. *Philos. Trans. R. Soc. Lond. B Biol. Sci.* 366:3498–3507.

Piel, M., and P.T. Tran. 2009. Cell shape and cell division in fission yeast. *Curr. Biol.* 19:R823–R827. http://dx.doi.org/10.1016/j.cub.2009.08.012

Qiu, Y., L.D. Fairbanks, K. Rückermann, C.M. Hawrylowicz, D.F. Richards, B. Kirschbaum, and H.A. Simmonds. 2000. Mycophenolic acid-induced GTP depletion also affects ATP and pyrimidine synthesis in mitogen-stimulated primary human T-lymphocytes. *Transplantation.* 69:890–897. http://dx.doi.org/10.1097/00007890-200003150-00038

Sagot, I., B. Pinson, B. Salin, and B. Daignan-Fornier. 2006. Actin bodies in yeast quiescent cells: an immediately available actin reserve? *Mol. Biol. Cell.* 17:4645–4655. http://dx.doi.org/10.1091/mbc.E06-04-0282

Sajiki, K., M. Hatanaka, T. Nakamura, K. Takeda, M. Shimanuki, T. Yoshida, Y. Hanyu, T. Hayashi, Y. Nakaseko, and M. Yanagida. 2009. Genetic control of cellular quiescence in *S. pombe*. *J. Cell Sci.* 122:1418–1429. http://dx.doi.org/10.1242/jcs.046466

Sajiki, K., T. Pluskal, M. Shimanuki, and M. Yanagida. 2013. Metabolomic analysis of fission yeast at the onset of nitrogen starvation. *Metabolites.* 3:1118–1129. http://dx.doi.org/10.3390/metabo3041118

Samejima, I., P.C.C. Lourenço, H.A. Snaith, and K.E. Sawin. 2005. Fission yeast mto2p regulates microtubule nucleation by the centrosomin-related protein mto1p. *Mol. Biol. Cell.* 16:3040–3051. http://dx.doi.org/10.1091/mbc.E04-11-1003

Samejima, I., V.J. Miller, S.A. Rincon, and K.E. Sawin. 2010. Fission yeast Mto1 regulates diversity of cytoplasmic microtubule organizing centers. *Curr. Biol.* 20:1959–1965. http://dx.doi.org/10.1016/j.cub.2010.10.006

Sawin, K.E., and P. Nurse. 1998. Regulation of cell polarity by microtubules in fission yeast. *J. Cell Biol.* 142:457–471. http://dx.doi.org/10.1083/jcb.142.2.457

Sawin, K.E., and H.A. Snaith. 2004. Role of microtubules and tea1p in establishment and maintenance of fission yeast cell polarity. *J. Cell Sci.* 117:689–700. http://dx.doi.org/10.1242/jcs.00925

Sawin, K.E., and P.T. Tran. 2006. Cytoplasmic microtubule organization in fission yeast. *Yeast.* 23:1001–1014. http://dx.doi.org/10.1002/yea.1404

Sawin, K.E., P.C.C. Lourenco, and H.A. Snaith. 2004. Microtubule nucleation at non-spindle pole body microtubule-organizing centers requires fission yeast centrosomin-related protein mod20p. *Curr. Biol.* 14:763–775. http://dx.doi.org/10.1016/j.cub.2004.03.042

Shah, K.H., R. Nostramo, B. Zhang, S.N. Varia, B.M. Klett, and P.K. Herman. 2014. Protein kinases are associated with multiple, distinct cytoplasmic granules in quiescent yeast cells. *Genetics.* 198:1495–1512. http://dx.doi.org/10.1534/genetics.114.172031

Snaith, H.A., and K.E. Sawin. 2003. Fission yeast mod5p regulates polarized growth through anchoring of tea1p at cell tips. *Nature.* 423:647–651. http://dx.doi.org/10.1038/nature01672

Su, S.S., Y. Tanaka, I. Samejima, K. Tanaka, and M. Yanagida. 1996. A nitrogen starvation-induced dormant G_0 state in fission yeast: the establishment from uncommitted G_1 state and its delay for return to proliferation. *J. Cell Sci.* 109:1347–1357.

Subramanian, R., and T.M. Kapoor. 2012. Building complexity: insights into self-organized assembly of microtubule-based architectures. *Dev. Cell.* 23:874–885. http://dx.doi.org/10.1016/j.devcel.2012.10.011

Tapia, H., and K.A. Morano. 2010. Hsp90 nuclear accumulation in quiescence is linked to chaperone function and spore development in yeast. *Mol. Biol. Cell.* 21:63–72. http://dx.doi.org/10.1091/mbc.E09-05-0376

Tischer, C., D. Brunner, and M. Dogterom. 2009. Force- and kinesin-8-dependent effects in the spatial regulation of fission yeast microtubule dynamics. *Mol. Syst. Biol.* 5:250. http://dx.doi.org/10.1038/msb.2009.5

Tran, P.T., L. Marsh, V. Doye, S. Inoué, and F. Chang. 2001. A mechanism for nuclear positioning in fission yeast based on microtubule pushing. *J. Cell Biol.* 153:397–411. http://dx.doi.org/10.1083/jcb.153.2.397

Unsworth, A., H. Masuda, S. Dhut, and T. Toda. 2008. Fission yeast kinesin-8 Klp5 and Klp6 are interdependent for mitotic nuclear retention and required for proper microtubule dynamics. *Mol. Biol. Cell.* 19:5104–5115. http://dx.doi.org/10.1091/mbc.E08-02-0224

Valiron, O., I. Arnal, N. Caudron, and D. Job. 2010. GDP-tubulin incorporation into growing microtubules modulates polymer stability. *J. Biol. Chem.* 285:17507–17513. http://dx.doi.org/10.1074/jbc.M109.099515

van der Vaart, B., A. Akhmanova, and A. Straube. 2009. Regulation of microtubule dynamic instability. *Biochem. Soc. Trans.* 37:1007–1013. http://dx.doi.org/10.1042/BST0371007

Vavylonis, D., J.-Q. Wu, S. Hao, B. O'Shaughnessy, and T.D. Pollard. 2008. Assembly mechanism of the contractile ring for cytokinesis by fission yeast. *Science.* 319:97–100. http://dx.doi.org/10.1126/science.1151086

Venkatram, S., J.J. Tasto, A. Feoktistova, J.L. Jennings, A.J. Link, and K.L. Gould. 2004. Identification and characterization of two novel proteins affecting fission yeast γ-tubulin complex function. *Mol. Biol. Cell.* 15:2287–2301. http://dx.doi.org/10.1091/mbc.E03-10-0728

Venkatram, S., J.L. Jennings, A. Link, and K.L. Gould. 2005. Mto2p, a novel fission yeast protein required for cytoplasmic microtubule organization and anchoring of the cytokinetic actin ring. *Mol. Biol. Cell.* 16:3052–3063. http://dx.doi.org/10.1091/mbc.E04-12-1043

Wade, R.H. 2009. On and around microtubules: an overview. *Mol. Biotechnol.* 43:177–191. http://dx.doi.org/10.1007/s12033-009-9193-5

Wei, W., P. Nurse, and D. Broek. 1993. Yeast cells can enter a quiescent state through G1, S, G2, or M phase of the cell cycle. *Cancer Res.* 53:1867–1870.

West, R.R., T. Malmstrom, C.L. Troxell, and J.R. McIntosh. 2001. Two related kinesins, *klp5*$^+$ and *klp6*$^+$, foster microtubule disassembly and are required for meiosis in fission yeast. *Mol. Biol. Cell.* 12:3919–3932. http://dx.doi.org/10.1091/mbc.12.12.3919

Woods, A., T. Sherwin, R. Sasse, T.H. MacRae, A.J. Baines, and K. Gull. 1989. Definition of individual components within the cytoskeleton of *Trypanosoma brucei* by a library of monoclonal antibodies. *J. Cell Sci.* 93:491–500.

Yamashita, A., M. Sato, A. Fujita, M. Yamamoto, and T. Toda. 2005. The roles of fission yeast ase1 in mitotic cell division, meiotic nuclear oscillation, and cytokinesis checkpoint signaling. *Mol. Biol. Cell.* 16:1378–1395. http://dx.doi.org/10.1091/mbc.E04-10-0859

Zheng, L., C. Schwartz, L. Wee, and S. Oliferenko. 2006. The fission yeast transforming acidic coiled coil–related protein Mia1p/Alp7p is required for formation and maintenance of persistent microtubule-organizing centers at the nuclear envelope. *Mol. Biol. Cell.* 17:2212–2222. http://dx.doi.org/10.1091/mbc.E05-08-0811

Zimmerman, S., and F. Chang. 2005. Effects of γ-tubulin complex proteins on microtubule nucleation and catastrophe in fission yeast. *Mol. Biol. Cell.* 16:2719–2733. http://dx.doi.org/10.1091/mbc.E04-08-0676

Laporte et al., http://www.jcb.org/cgi/content/full/jcb.201502025/DC1

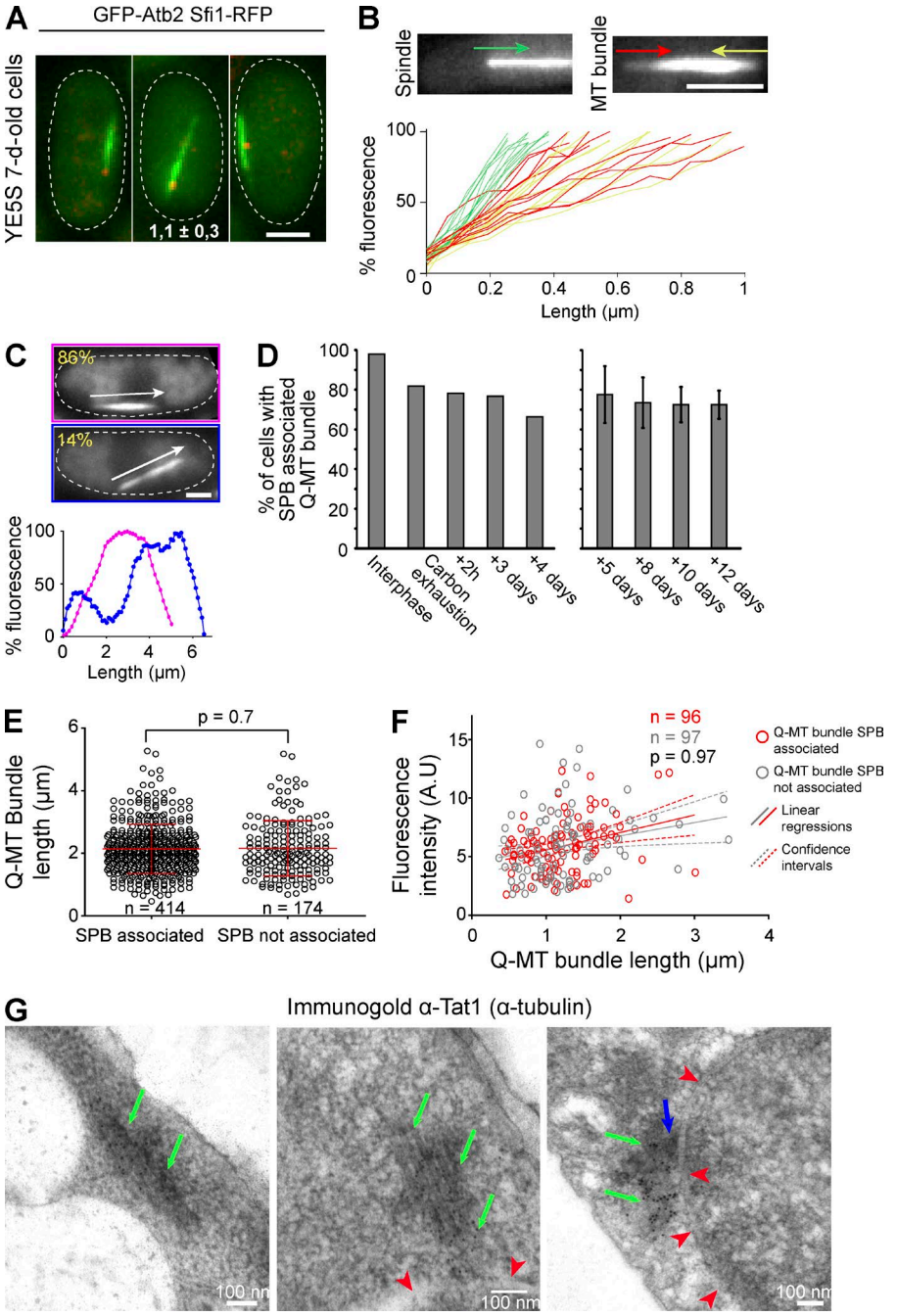

Figure S1. **Properties and detection of the Q-MT bundle by EM.** (A) WT cells expressing GFP-Atb2 (green) and Sfi1-RFP (red) grown for 7 d in YE5S+A display a Q-MT bundle. The mean number of MT bundles per cell is indicated. (B) Fluorescence line scan intensity reveals the tapered shape of the Q-MT bundle. Fluorescence intensity line scan at Q-MT bundle extremities (standardized slopes) are shown (red and yellow). For comparison, the slopes measured for mitotic spindle extremities are shown (green); $n = 20$ for each category. (C) Q-MT bundle can display internal thickness variation. Representative images and the corresponding fluorescence line scan analysis show that the Q-MT thickness may vary. The relative percentage of each kind of Q-MT bundle in the cell population is shown (N = 2 experiments and $n > 100$). Bars, 2 µm. (D) Evolution of the number of Q-MT bundles associated with the SPB as a function of time before or after carbon exhaustion. Error bars are SDs. The data in the left graph are from a single representative experiment out of three repeats. (E and F) Q-MT bundles have the same length (E, red line: mean and SD) and the same intensity (F, red and gray lines: linear regressions), regardless of whether or not they are SPB associated. Numbers of Q-MT bundles analyzed and p-values are indicated. (G) Q-MT bundles detected in 7-d-old WT quiescent cells by immuno-EM using gold-labeled anti–α-tubulin antibodies. Green arrows, MTs; blue arrow, SPB; red arrowheads, nuclear membrane.

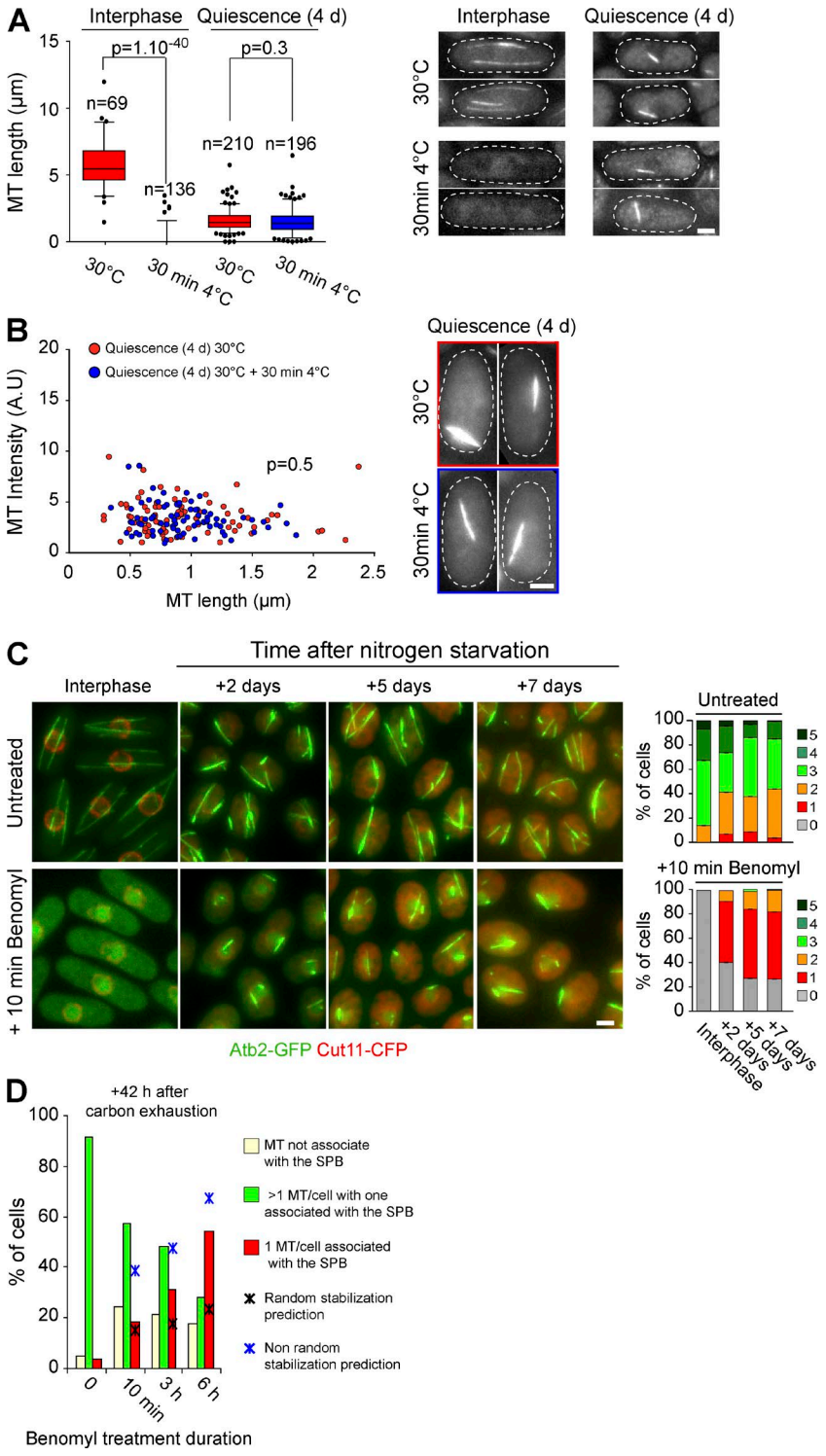

Figure S2. **Q-MT bundle resistance to cold treatment and its formation upon nitrogen starvation.** (A and B) Interphase and quiescent cells (4 d) expressing GFP-Atb2 were cold treated (4°C) for 30 min. (A) MT lengths were measured after cell fixation. (B) Fluorescence intensity as a function of the bundle length was plotted in live cells. For A and B, representative cells are shown and p-values are indicated. The data shown are from a single representative experiment (n = 80) out of three repeats. (C) MTs are stabilized upon nitrogen starvation. Proliferating and nitrogen-starved WT cells expressing GFP-Atb2 Cut11-CFP were incubated 10 min or not with benomyl. Representative cells are shown. Graphs display MT bundle numbers per cell over time. Bars, 2 µm. (D) MT stabilization is biased toward the SPB-associated MT bundle. Quantification of the MT bundle associated with the SPB before and after the indicated benomyl treatment. Cells were analyzed 42 h after carbon starvation (n > 170 per time point) from a single experiment. See Fig. 3 E for a detailed legend.

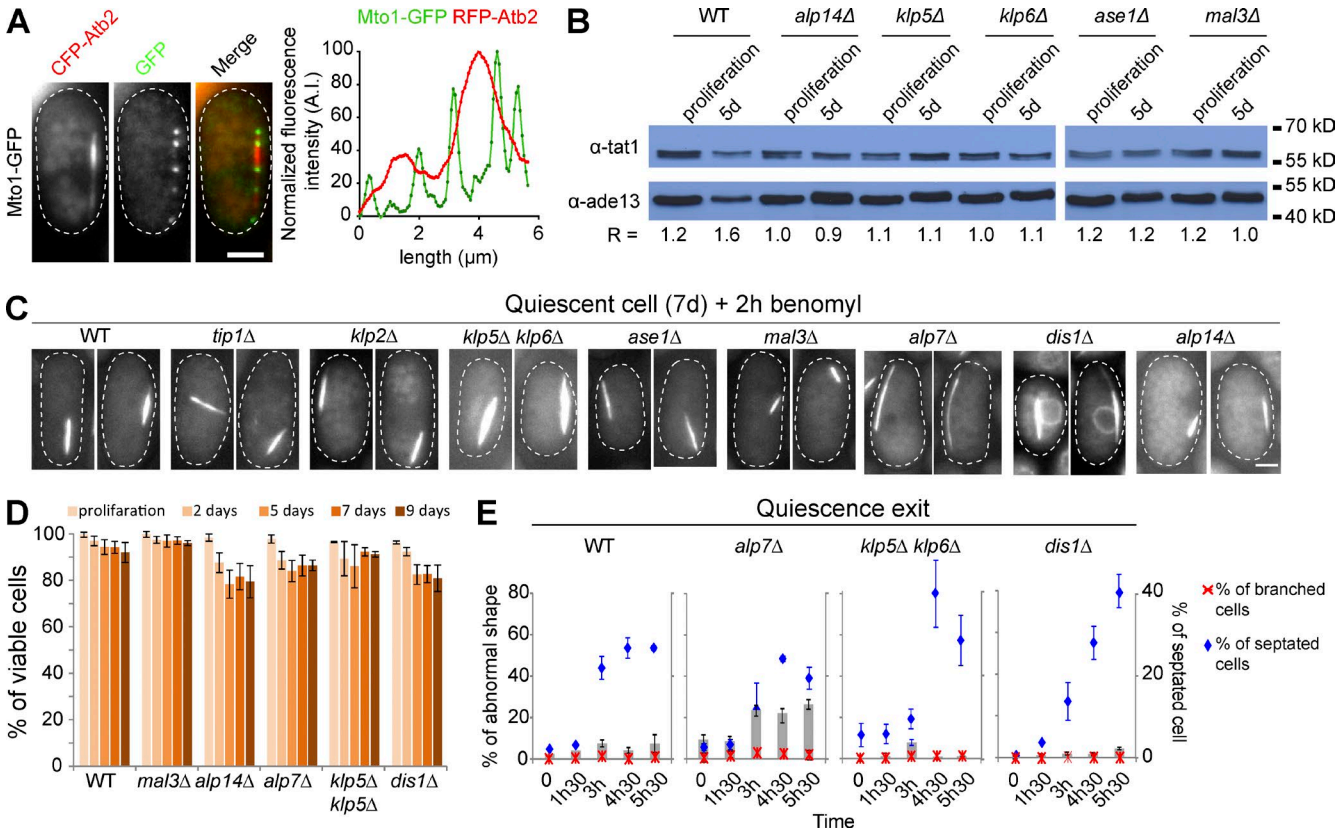

Figure S3. **Localization of Mto1-GFP and phenotypes of MAP mutants in quiescence.** (A) Mto1 localized as dots along the Q-MT bundle. Cells expressing RFP-Atb2 and Mto1-GFP were grown for 7 d and imaged. A representative line scan along the Q-MT bundle is shown out of four experimental repeats. (B) The relative steady-state amount of α-tubulin isoforms did not vary between WT and mutant cells studied. Western blots were done on proliferating and quiescent cells (5 d) using anti-Tat1 antibodies. Antibody against the budding yeast Ade13, the homologue of fission yeast Ade8, was used to normalize the tubulin signal. R is the ratio of tubulin to Ade13 intensity signals. (C) Deleting various MAPs did not affect Q-MT bundle stability. 7-d-old cells were treated with benomyl and the presence of the Q-MT bundle was analyzed. Representative cells are shown. All cells express GFP-Atb2 except the *dis1Δ* strain (F303) that coexpresses GPP-Atb2 and Cut11-GFP. In this strain, both the nuclear membrane and MT are thus detected. Bars, 2 μm. (D and E) Deleting various MAPs did not affect cell viability in quiescence or quiescence exit efficiency. (D) Cell viability was scored using methylene blue staining. (E) 4-d-old quiescent cells were inoculated in YPDA. Septum formation and cell shape were analyzed as a function of time after refeeding. The percentage of cells with an abnormal shape are shown as gray bars. For all graphs, SDs are indicated.

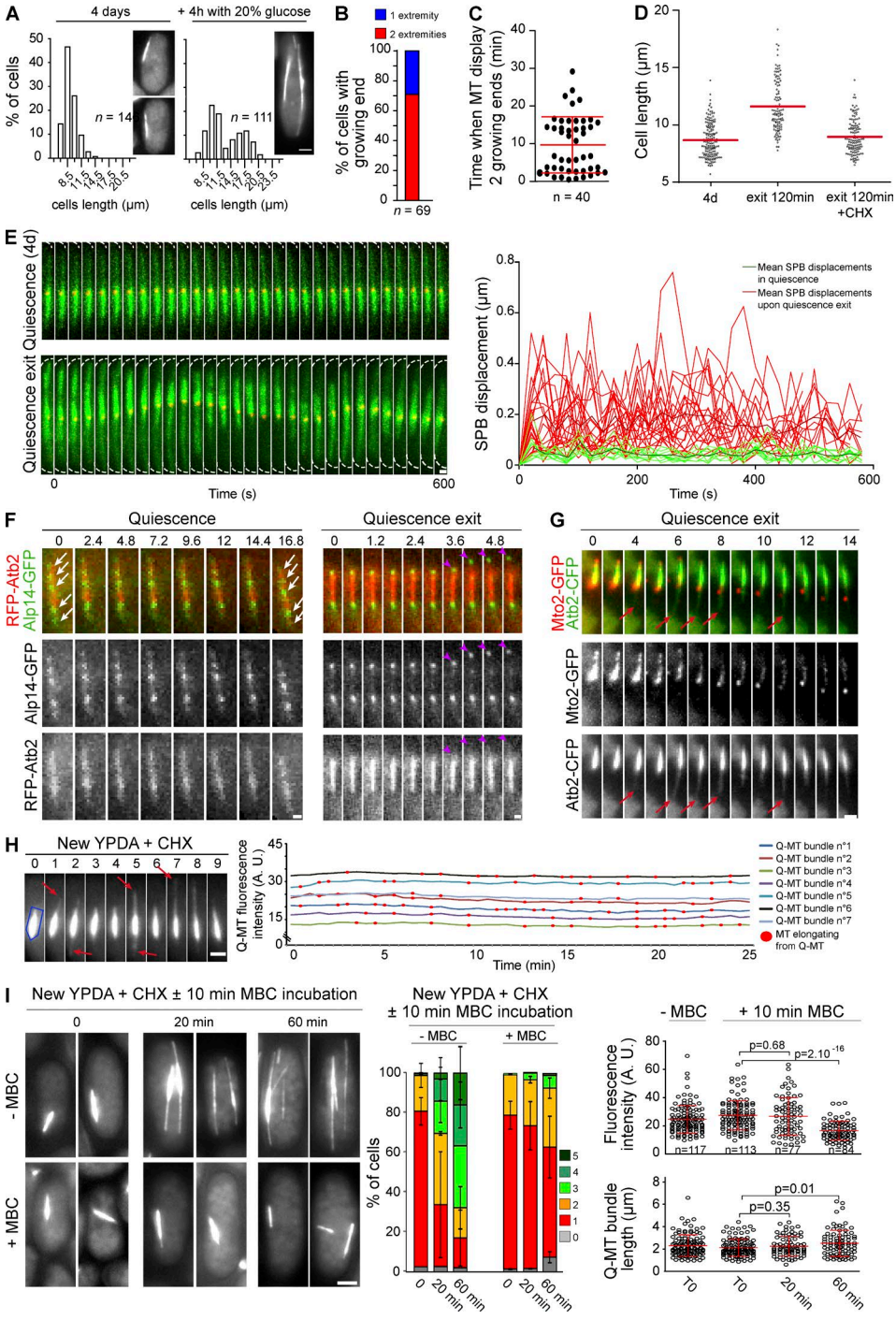

Figure S4. **Q-MT bundle properties upon quiescence exit.** (A) Glucose addition onto a 4-d-old YPDA culture is enough to induce cell regrowth. Cell length is indicated before and after glucose addition. Representative cells are shown. Bar, 2 µm. (B and C) The Q-MT bundle elongates from both extremities upon quiescence exit. (B) Percentage of cells with a Q-MT bundle growing from a one or both ends during the first 30 min after cell refeeding. (C) Time needed for growth at both extremities upon quiescence exit. (D) CHX inhibits cell growth upon quiescence exit. Cell length was measured before and after quiescence exit in the presence or absence of CHX. In B–D, WT cells expressing GFP-Atb2 grown 5 d in YPDA were used. (E) The Q-MT bundle stays attached to the SPB upon quiescence exit. Time-lapse movies in quiescence (4 d, top) and upon quiescence exit (bottom) are shown. The cell wall is indicated as a white dashed line. The graph represents the individual SPB displacement (thin lines) as a function of time after refeeding. Bold lines are the mean values. *n* = 24 and 11 SPBs, respectively, followed in 4-d-old cells exiting quiescence or not, from a single experiment. Bar, 1 µm. (F) In quiescent cells (5 d), Alp14 dots are immobile on the Q-MT bundle (left, white arrows), whereas they follow the MT growing extremities upon quiescence exit (right, pink arrowhead). (G) Mto2 does not follow the MT growing tip (red arrow) upon quiescence exit. In F and G, time-lapse movies are presented. Time is in minutes. Bars, 1 µm. (H) Fluorescence intensity measurements of the Q-MT bundle (blue outline) upon quiescence exit. Experiments were done in the presence of CHX to avoid de novo tubulin synthesis. Red arrows show MT growing from the Q-MT bundle. The graph displays the variation of the Q-MT bundle fluorescence intensity as a function of time after cell refeeding. Red circles mark MT elongating from the Q-MT bundle. (I) The Q-MT bundle disassembles upon quiescence exit. 6-d-old WT cells expressing GFP-Atb2 were refeed with YPDA+CHX and, at indicated time points, were incubated with MBC for 10 min. Representative cells are shown. Graphs represent, respectively, the number of MT structures per cell, their intensity, and their length. Number of cells, SEM, and p-values are indicated. Bars, 2 µm.

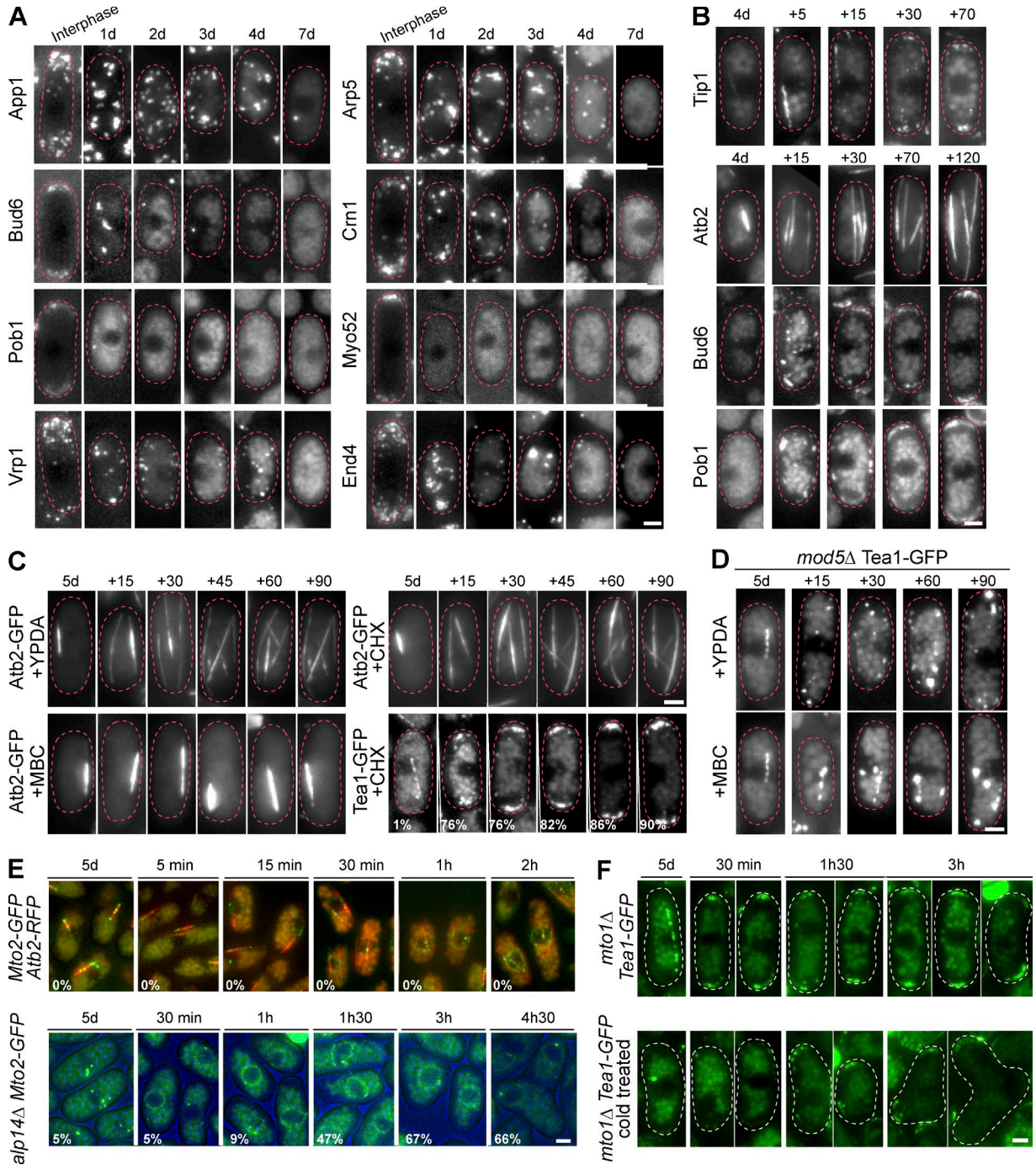

Figure S5. **Polarity marker localization upon quiescence entry and exit in WT and mutants.** (A) Polarity markers relocalize upon quiescence entry. Cells expressing the indicated protein fused to GFP are shown. (B) Polarity markers rapidly relocalize at cell tips upon quiescence exit. (C) Control experiments for Fig. 7 A. MT regrowth and Tea1 cell tip relocalization occur in the presence of CHX but not in the presence of MBC. Numbers indicate the percentage of cells with polarized Tea1-GFP. (D) Mod5 is critical to localize Tea1 at the cell tip upon quiescence exit in the presence of MBC. For B–D, time is in minutes. (E, top) Localization of RFP-Abt2 and Mto2-GFP in WT cells upon quiescence exit. (bottom) Mto2-GFP localization in *alp14Δ* cells upon quiescence exit. Percentage of cells with an abnormal shape are indicated. (F) 5-d-old *mto1Δ* cells expressing Tea1-GFP were cold treated, and after complete MT disappearance (17 h) cells where shifted back to 30°C. Tea1 localization was then imaged upon quiescence exit. Bars, 2 µm.

Table S1. ***S. pombe* strains used in this study**

Strain	Genotype	Source
F5	*h⁻ Crn1-GFP; ade6 ; leu1; ura4*	Pelham and Chang, 2001
F7	*h⁻ GFP-atb2-kanR, Cut11-3mRFP-HphR, Sfi1-CFP-NatR, leu1⁻, ura4-D18*	Sato et al., 2009
F9	*h⁻ Vrp1-GFP-kanMX6; ade6-M216; leu1-32; ura4-D18; his3-D1*	Sirotkin et al., 2005
F10	*h⁻ Arp5-mGFP-kanMX6; ade6; leu1-32; ura4-D18; his3-D1*	Sirotkin et al., 2005
F11	*Fim1-mCFP-kanMX; Acp2-YFP-kanMX6 ade6-M210; leu1-32; ura4-D18*	Sirotkin et al., 2005
F12	*h⁺ App1-mGFP-kanMX6; ade6-M210; leu1-32; ura4-D18; his3-D1*	Sirotkin et al., 2005
F14	*h⁺ End4-mGFP-kanMX6. ade6-M210; leu1-32; ura4-D18; his3-D1*	Sirotkin et al., 2005
F21	*h⁻ fim1-GFP(S65T)-kanMX6*	Wu et al., 2001
F185	*h⁻ tea1::ura4+; ura4-D18; ade6-M216*	Snaith and Sawin, 2003
F186	*h⁺ Tea1-GFP::kanMX; ura4-D18; leu1-32; ade6-M216*	Snaith and Sawin, 2003
F187	*h⁻ mod5::kanMx; tea1-GFP::kanMX; ura4-D18; leu1-32; ade6-M210*	Snaith and Sawin, 2003
F192	*h⁻ bud6-GFP::kanMx6, leu1-32, ura4D-18*	Martin et al., 2007
F195	*h⁺ sec8-GFP::ura4, leu1-32, ura4-D18*	Wang et al., 2002
F198	*h⁺ CRIB-GFP::ura (Sc GIC2:3XGFP), leu1-32*	Rincón et al., 2009
F200	*h⁻ GFP-pob1::ura, leu1-32, ura4D-18*	Rincón et al., 2009
F201	*h⁺ myo52-GFP::kanR, leu1-32, ura4D-18, lys3-D1*	Martin et al., 2007
F204	*h⁺ Exo70-GFP::kanR, leu1-32, ura4*	Estravís et al., 2011
F1	*972 h⁻*	ATCC 24843
F103	*mCherry-atb2::Hygro; mto2-GFP::KanR; leu1-31 ura4-D18*	This study
F107	*mCherry-atb2::Hygro; ase1-GFP::KanR; leu1-31 ura4-D18*	This study
F111	*h⁺ mCherry-atb2::Hygro mto1-GFP::KanR; leu1-31; ura4-D18; ade6-212*	This study
F123	*tip1::kanR; GFP-atb2::KanR; ura4-D18*	This study
F128	*h⁻ alp14::ura4; GFP-atb2::KanR, leu1-31, ura4-D18*	This study
F134	*h⁻ klp2-delta::ura4; GFP-atb2::KanR; leu1-31; ura4-D18 ;ade6-212*	This study
F164	*h⁺ Dis1-GFP-kanr; mCherry-atb2::Hygro; ura4-D18; leu1-31*	This study
F166	*h⁺ Tip1-GFP::kanR; leu1-32; ura4-D18; ade6-M216*	This study
F172	*h⁺ mCherry-atb2::Hygro; alp14-GFP::kanMX; leu1⁻; ura4-D18*	This study
F175	*h⁺ mCherry-atb2::Hygro; cls1-3GFP::kanMX; leu1⁻; ura4-D18*	This study
F178	*h⁻ Alp7-GFP-kanr; mCherry-atb2::Hygro; leu1⁻; ura4-D18*	This study
F180	*h⁻ alp7::ura4; GFP-atb2::KanR; ura4-D18; leu⁻, ade-M216*	This study
F211	*h⁺ GFP-atb2-kanR, Cut11-3mRFP-HphR, Sfi1-CFP-NatR*	This study
F215	*h⁺ alp14::ura4; GFP-atb2::KanR; ura4-D18; leu⁻; ade6⁻*	This study
F217	*h⁺ klp2-delta::ura4; GFP-atb2::KanR; ura4-D18; leu⁻; ade6⁻*	This study
F226	*ase1-delta::KanR; GFP-atb2::KanR; leu⁻; ura4-D18; ade6⁻*	This study
F231	*h⁺ klp6::ura4; klp5::ura4; GFP-atb2::KanR; leu1-31; ura4-D18; ade6⁻; his7⁻*	This study
F233	*h⁺ mto1-delta::ura4; GFP-atb2-kanR, Cut11-3mRFP-HphR, Sfi1-CFP-NatR; ade6-212; ura4-D18*	This study
F239	*h⁻ alp14::ura4; mto2-GFP::KanR; ura4⁻; leu⁻*	This study
F247	*h⁻ mal3-delta::his3, GFP-atb2::KanR; leu1-31, ura4-D18*	This study
F291	*h⁺ mto1-delta::ura4; Tea1-GFP::kanMX; ura4-D18; leu1-32; ade6-M216*	This study
F299	*h⁻ Dis1::KanR; GFP-atb2-kanR, Cut11-3mRFP-HphR; Sfi1-CFP-NatR; leu⁻*	This study
F303	*Dis1::KanMX6; cut11-GFP::natR; GFP-atb2::natR; ade6⁻; leu1⁻; ura4⁻*	Scheffler et al., 2015
F338	*alp14::ura4; GFP-atb2::KanR; leu1⁻; ura4⁻; ade6⁻*	This study
F340	*alp14::ura4; Tea1-GFP::kanMX; leu1⁻; ura4⁻; ade6⁻*	This study

References

Estravís, M., S.A. Rincón, B. Santos, and P. Pérez. 2011. Cdc42 regulates multiple membrane traffic events in fission yeast. *Traffic.* 12:1744–1758. http://dx.doi.org/10.1111/j.1600-0854.2011.01275.x

Martin, S.G., S.A. Rincón, R. Basu, P. Pérez, and F. Chang. 2007. Regulation of the formin for3p by cdc42p and bud6p. *Mol. Biol. Cell.* 18:4155–4167. http://dx.doi.org/10.1091/mbc.E07-02-0094

Pelham, R.J. Jr., and F. Chang. 2001. Role of actin polymerization and actin cables in actin-patch movement in *Schizosaccharomyces pombe*. *Nat. Cell Biol.* 3:235–244. http://dx.doi.org/10.1038/35060020

Rincón, S.A., Y. Ye, M.A. Villar-Tajadura, B. Santos, S.G. Martin, and P. Pérez. 2009. Pob1 participates in the Cdc42 regulation of fission yeast actin cytoskeleton. *Mol. Biol. Cell.* 20:4390–4399. http://dx.doi.org/10.1091/mbc.E09-03-0207

Sato, M., M. Toya, and T. Toda. 2009. Visualization of fluorescence-tagged proteins in fission yeast: the analysis of mitotic spindle dynamics using GFP-tubulin under the native promoter. *Methods Mol. Biol.* 545:185–203.

Scheffler, K., R. Minnes, V. Fraisier, A. Paoletti, and P.T. Tran. 2015. Microtubule minus end motors kinesin-14 and dynein drive nuclear congression in parallel pathways. *J. Cell Biol.* 209:47–58. http://dx.doi.org/10.1083/jcb.201409087

Sirotkin, V., C.C. Beltzner, J.-B. Marchand, and T.D. Pollard. 2005. Interactions of WASp, myosin-I, and verprolin with Arp2/3 complex during actin patch assembly in fission yeast. *J. Cell Biol.* 170:637–648. http://dx.doi.org/10.1083/jcb.200502053

Snaith, H.A., and K.E. Sawin. 2003. Fission yeast mod5p regulates polarized growth through anchoring of tea1p at cell tips. *Nature.* 423:647–651. http://dx.doi.org/10.1038/nature01672

Wang, H., X. Tang, J. Liu, S. Trautmann, D. Balasundaram, D. McCollum, and M.K. Balasubramanian. 2002. The multiprotein exocyst complex is essential for cell separation in *Schizosaccharomyces pombe*. *Mol. Biol. Cell.* 13:515–529. http://dx.doi.org/10.1091/mbc.01-11-0542

Wu, J.Q., J. Bähler, and J.R. Pringle. 2001. Roles of a fimbrin and an α-actinin-like protein in fission yeast cell polarization and cytokinesis. *Mol. Biol. Cell.* 12:1061–1077. http://dx.doi.org/10.1091/mbc.12.4.1061